U.S. Department of Energy

Oakland Operations Office, Oakland, California 94612

Lawrence Livermore National Laboratory

University of California, Livermore, California 94550

UCRL-AR-136098

Evaluating the Application of Electroosmosis to the Cleanup of Fine-Grained Sediments in Contaminant Plume Source Areas at Lawrence Livermore National Laboratory

Authors

Walt W. McNab, Jr.
Roberto Ruiz

December 1999

Environmental Protection Department

Environmental Restoration Division

Work performed under the auspices of the U. S. Department of Energy by Lawrence Livermore National Laboratory under Contract W-7405-Eng-48.

UCRL-AR-136098

Evaluating the Application of Electroosmosis to the Cleanup of Fine-Grained Sediments in Contaminant Plume Source Areas at Lawrence Livermore National Laboratory

Authors

Walt W. McNab, Jr.
Roberto Ruiz

December 1999

Environmental Protection Department
Environmental Restoration Division

Acknowledgments

This report presents a summary of the Qualification Phase tests of electroosmosis conducted at Lawrence Livermore National Laboratory (LLNL) as part of the Phased Source Area Contaminant Remediation effort funded as an Accelerated Site Technology Deployment Initiative through EM-50. Kim Abbott, Technical Program Officer for the EM-50 Environmental Programs Division, has been instrumental in supporting this work. In addition, the contributions of a number of individuals from LLNL whom have supported the project on a technical level are gratefully acknowledged, including:

Bob Bainer
Nerine Cherepy
William Daily, Sr.
Zafer Demir
Brenda Ekwurzel
Bryant Hudson
John Karachewski
P.J. Lyra
George Metzger
Mark Montgomery
Jean Moran
Charles Noyes
Tristan Pico
Abe Ramirez

Purpose and Scope

The groundwater pump-and-treat strategy employed by Lawrence Livermore National Laboratory (LLNL) to address groundwater contamination by chlorinated volatile organic compounds (CVOCs) has succeeded in controlling plume migration offsite from the LLNL Livermore Site and has resulted in significant contaminant mass removal. Nevertheless, the source areas which feed the CVOC plumes are in many cases characterized by relatively high concentrations of contaminants in fine-grained (i.e., low permeability) sediments. Because such silty and clayey sediments do not yield contaminants effectively by hydraulic pumping, transport of contaminants into mobile portions of the plume is diffusion-limited and thus could require decades or even centuries for purging. As a consequence, the overall time required to operate the pump-and-treat systems, and hence the associated cumulative costs, may be extensive.

The phenomenon of electroosmosis provides a means by which the removal of CVOCs from fine-grained sediments can be greatly expedited. Briefly, electroosmosis entails the movement of pore water under the influence of an electric field, as opposed to that under a hydraulic gradient. This movement is a result of the coulomb attraction of the diffusive double layer (the cloud of water molecules and positively-charged ions that forms over the negatively-charged surfaces of clay minerals) toward the cathode; viscous drag tends to pull the remaining pore water in the same direction. The flux of water associated with electroosmosis, q, is proportional to the voltage gradient, $\nabla\phi$,

$$q = \frac{-k_{eo}}{n}\nabla\phi \qquad \text{(Eq.-1)}$$

where k_{eo} is the electroosmotic conductivity and n the porosity. In principle, the electroosmotic conductivity is not a true constant of the material because it depends on a number of factors (e.g. ζ-potential) which may vary with pH and other variables. However, the k_{eo} is nonetheless useful for engineering design purposes (Mitchell, 1993).

Electroosmosis was first explored as a means for de-watering clays for purposes of soil stabilization (e.g., Casagrande, 1952). In recent years, the potential of electroosmosis for removing contaminants from fine-grained sediments has been explored in both laboratory studies and field scale demonstrations (Hamed et al., 1991, Bruell et al., 1992, Segall and Bruell, 1992, Acar and Alshawabkeh, 1993, Lageman, 1993, Probstein and Hicks, 1993, Shapiro et al., 1993). Recently, the DOE-funded Lasagna™ Project at the Paducah Gaseous Diffusion Plant employed electroosmosis to transport TCE to activated carbon or iron filing treatment zones within the electric field, resulting in an estimated removal efficiency of 98% in 3 pore volumes (Athmer et al., 1997). With regard to the LLNL Livermore Site in particular, previous bench-top tests using site soil samples have demonstrated that electroosmosis can increase the effective hydraulic conductivity of fine-grained soils by two orders-of-magnitude (Pamukcu and Pervizpour, 1998).

LLNL has chosen to apply electroosmosis at selected locations as part of a larger effort to focus cleanup efforts on CVOC plume source areas. Prior to full-scale deployment of the electroosmosis technology (Deployment Phase), a testing program has been conducted using limited two- and

four-electrode arrays installed in groundwater wells at the former Treatment Facility F (TFF) area at the LLNL Livermore Site (Qualification Phase). The hydrostratigraphic units targeted by these operational tests are impacted primarily by fuel hydrocarbons and not CVOCs and have been granted No-Further-Action-Status by the site regulatory stakeholders owing to the success of prior remediation efforts (dynamic steam stripping, pump-and-treat, soil vapor extraction, bioremediation) in the area. Hence, the purpose of the Qualification Phase tests of electroosmosis was not to facilitate further cleanup in the area, but rather to address a number of key operational issues:

- Measurement of soil bulk electrical conductivity and electroosmotic conductivity to validate and calibrate mathematical screening models to be used in the Deployment Phase. This involved (1) the development of a semi-analytical screening model for quantifying electroosmotic fluxes in response to an electric field, (2) direct measurement of soil bulk electrical conductivity, (3) indirect measurements of induced electroosmotic flux, and (4) comparison of data measured in the field to those observed in bench-top laboratory tests[1] conducted on TFF soil cores as well as to values published in the literature.
- Identification of method(s) for controlling the extreme pH values that may be near the electrodes as a result of the electrolysis of water.
- Assessment of the stability of the electric current under a constant voltage difference.
- Identification of any unforeseen technical problems specific to the equipment used in the tests or the LLNL subsurface environment that could present adverse effects in the Deployment Phase.

The methods and findings of the operational tests conducted at TFF are discussed in this report. In general, the tests have shown that the sediments in the TFF area are typical in terms of soil electrical and electroosmotic conductivities reported in the literature, that measurable electroosmotic fluxes can be induced using readily available equipment and reasonable quantities of electric power, and that the observed electroosmotic fluxes can be quantified effectively using a relatively simple semi-analytical screening model. Moreover, application of the screening model to the more robust electrode geometries of the Deployment Phase indicates a dramatic improvement in contaminant removal rates from silty and clayey materials in comparison to hydraulic pumping, using physical parameters measured at TFF from field and laboratory tests. Because the alluvial sediments found across the LLNL Livermore Site are comprised of similar lithological materials and exhibit similar groundwater geochemical signatures, the soils in the TFF area are presumably a reasonable surrogate for soils elsewhere on site.

Test Area Features and Equipment

Hydrogeology

The TFF area, contaminated by fuel hydrocarbons from former underground storage tanks, has been the subject of extensive prior remediation and investigation efforts since the early 1990s (e.g., Happel et al., 1996). Cleanup technologies included dynamic underground steam stripping, electrical resistive heating, soil vapor extraction, groundwater extraction, and passive bioremediation. As a consequence of the subsurface investigations associated with these activities, the hydrostratigraphy in the TFF area has been well characterized on a local scale. Of particular

[1] Conducted as part of a separate study, funded by LLNL LDRD.

interest is a zone of predominantly fine-grained sediments located between 110 and 120 feet below ground surface at the base of hydrostratigraphic unit HSU-3A (Happel et al., 1996). An investigatory well, W-1115, installed in 1995 as part of a passive bioremediation study revealed that these fine-grained sediments harbored relatively high residual concentrations of fuel hydrocarbons (Tables 1A and 1B) and thus constituted an ideal model of a fine-grained source area for CVOC plumes elsewhere on site (Figure 1). For this reason, this location was selected for the Qualification Phase electroosmosis operational tests.

Three additional wells – W-1513, W-1514, and W-1515 – were installed in the spring of 1999, that, taken together with W-1115, created a 10-ft by 10-ft grid to house the electrode array (Figure 2). During drilling, soil cores were collected for bench-top testing (electroosmotic conductivity, hydraulic conductivity, electrical conductivity, clay mineralogy). All of the wells share similar screened intervals, approximately from 110 feet to 120 feet. Lithologic and geophysical logs, similar among each of the wells, suggest that these wells are screened primarily across fine-grained sediments, although with some sandy intervals also present.

An aquifer test conducted by pumping W-1514, with the other three wells in the array used as monitor wells, indicated a high degree of hydraulic communication between the wells, with a relatively high hydraulic conductivity across the screened zone (Table 2). However, separate hydraulic conductivity measurements in bench-top tests conducted on soil cores collected from W-1513 indicated very low hydraulic conductivities in the silty/clayey materials (~ 1×10^{-8} cm/s, N. Cherepy, personal communication, 1999). Thus, the relatively high hydraulic conductivities suggested by the pumping tests are presumably reflective only of the sandy intervals.

Equipment

The equipment configuration installed in the TFF area to support the electroosmosis tests is shown on Figure 3. Two 10-ft (3 m) by 3-in (7.6-cm) diameter graphite electrodes were installed within the screened intervals of wells W-1514 and W-1515 (6-in, or 15.2-cm, diameter well bores); two 10-ft (3-cm) by 2-in (5.1-cm) diameter carbon steel electrodes[2] were installed in wells W-1115 and W-1513 (4-in, or 10.2-cm, diameter well bores). Two 100 V, 10-amp power supplies provided power to the electrodes. Variable speed submersible pumps were placed in each of the wells housing the cathodes, W-1514 and W-1515. The pumps in these two wells were plumbed to a set of instrumented manifolds. The treatment system for the extracted groundwater consisted of a series of granular activated carbon beds. Water was pumped from each cathode well at 1 gal/min (3.9 L/min), with a combined flow stream through the treatment unit at 2 gal/min (7.8 L/min). After treatment the water was re-injected into the anode wells (W-1115 and W-1513). Sample ports were located at the influent and effluent streams and between the treatment units.

The system was designed to operate on a continuous basis and to automatically shut down in an abnormal event (e.g., pump failure, low water level). Electrode voltage and current and water flow were continuously monitored and controlled thru Opto-22 hardware and Bridgeview software. Water pH, temperature, and conductivity were also monitored and recorded continuously using

[2] The carbon steel electrodes were replaced in the long-term tests with graphite electrodes.

Bridgeview software. In addition, gases generated from the electrolysis of the groundwater in the well bores were periodically monitored to assure against an explosion hazard.

Test Results

Soil Electrical Conductivity Measurements

Electrical conductivity/resistivity was measured using a four electrode array, with a voltage difference applied across the electrodes in wells W-1513 and W-1515 while the passive electrodes in W-1115 and W-1514 were used to monitor the voltage potential distribution. The advantage of measuring the voltage difference between the passive electrodes, as opposed to the active ones, is that voltage drops associated with surface chemistry effects, as well as those associated with the well bore water and the PVC well casing, could be avoided. With the chosen electrode geometry, the two passive electrodes would not lie on an equipotential line, so that a voltage difference could be measured (Figure 4).

The measured electrical currents and passive electrode voltage differences as a function of applied voltage across the active electrodes are shown on Table 3. Because the two passive electrodes consisted of unlike materials (carbon steel and graphite), a DC offset associated with oxidation-reduction reactions of approximately 0.683 V was subtracted from the data to yield the correct voltage difference. Based on the observed passive electrode voltage differences and the electrode geometry, a semi-analytical model of the potential distribution was used to calculate the soil bulk electrical conductivity (see discussion under "Modeling"). The resulting estimated value, approximately 0.13 siemens/m, is well within the typical range reported for soils (0.01 to 1 S/m, Mitchell, 1993). Electrical conductivity was also measured in the laboratory for a single soil core collected from the W-1513 soil boring and was estimated to range between approximately 0.06 – 0.09 siemens/m (N. Cherepy, personal communication, 1999).

Measurements of transfer resistance between various combinations of electrodes generally all indicated values on the order of 0.1 Ω (W. Daily, personal communication, 1999), indicating, as expected, that there are no abrupt horizontal discontinuities in the resistivity field within the electrode array.

pH Effects and Control Strategy

The electrolysis of water by a DC current under a sufficient voltage produces acidic conditions at the anode and alkaline conditions at the cathode, respectively:

$$2H_2O \rightarrow O_2 + 4H^+ + 4e^- \qquad \text{(Eq.-2)}$$

$$2H_2O + 2e^- \rightarrow H_2 + 2OH^- \qquad \text{(Eq.-3)}$$

These reactions can exert a number of effects on electroosmosis. The surface chemical properties of clay minerals (e.g., cation exchange capacity, ζ-potential, etc) are dependent on pH, so the electroosmotic conductivity, and to a lesser extent the electrical conductivity, can be influenced in the

vicinity of both electrodes by these reactions. Furthermore, acidic conditions near the anode can result in the mobilization of trace metals, either by cation exchange or by the dissolution of oxyhydroxide mineral phases. Finally, the high pH in the vicinity of the cathode may induce mineral precipitation reactions, such as the formation of calcium carbonate (calcite):

$$Ca^{2+} + HCO_3^- + OH^- \rightarrow CaCO_3(s) + H_2O \qquad \text{(Eq.-4)}$$

This reaction is of particular concern with regard to groundwater at the LLNL Livermore Site, where the groundwater geochemical composition is slightly supersaturated with calcite. Any rise in pH would be expected to result in precipitation of calcite, as is frequently observed in groundwater treatment system air strippers where a pH rise is caused by de-gassing of dissolved CO_2. For the electroosmosis system, calcite precipitation can be problematic because of the potential to cover the cathode(s) with a non-conductive material, thus disrupting the flow of electric current, as well as the potential for clogging of the well screen.

The response of the pH in the cathode well bore water during a short-term test (50 V difference applied between the electrodes in W-1514 and W-1515) is shown on Figure 5. Also illustrated are the simulated responses of area groundwater (as indicated by an analysis of a W-1115 water sample collected in 1995) to titration with OH-, used as a surrogate for the electrolysis reaction, according to the U.S.G.S. PHREEQC model (Parkhurst, 1995). Two scenarios were included in the model, one with calcite precipitation in response to the pH increase and one without. The observed pH data appear to follow the latter scenario up to a pH of approximately 8.7, after which the rate of pH increase abruptly slows. This suggests a possible kinetic limitation to calcite dissolution up to a certain pH before precipitation accelerates. However, this is only one possible interpretation. Other factors may be in effect as well, including the mixing of ions between the well bore and the surrounding formation water, that may also play a role. Following the test, both electrodes were removed for inspection. While the anode showed no visible difference in appearance in comparison to an unused electrode, the cathode appeared to be covered with a thin layer calcium carbonate (confirmed by effervescence upon application of dilute HCl).

Despite the presence of calcite on the cathode surface, a graph of the measured electric current across the electrodes indicates no particular relationship to the pH (i.e., the decline in current is continuous during the test and does not change as the pH rise slows after 60 minutes). The decline in current is apparently related to other factors (see discussion under “Long-Term System Performance”). Nevertheless, the calcite precipitation problem at the cathode cannot be permitted to continue indefinitely. As water is drawn through the system, calcite would continue to precipitate unabated, eventually leading to a shut down of the operation. Hence, a strategy for controlling pH warranted development. One option is to titrate an acid and a base into the cathode and anode well bore waters, respectively, to maintain neutrality. This option is maintenance-intensive and can be difficult to establish using in-line control loops. A second strategy is to periodically reverse the polarity of the electrodes, temporarily acidifying the previously alkaline environment of the cathode well bore to facilitate dissolution of the calcite. However, this option cannot be used as an exclusive means for controlling pH as it reverses the direction of electroosmotic flow and thus substantially reduces the overall contaminant removal efficiency.

A third option is to dilute the well bore water by hydraulic pumping from the sand fingers intercepted by the well screens. Assuming that each mole of electrons supplied to the cathode produces one mole of hydroxide ion (Eq.-3), the rate of hydroxide production, p_{OH}, via electrolysis may be given by,

$$p_{OH} = \frac{i}{F} \qquad \text{(Eq.-5)}$$

where *i* is the current and *F* the Faraday constant (96,500 coulombs/mol). At an applied current of 4 amps, for example, the corresponding rate of hydroxide production is equal to approximately 4.1 x 10^{-5} mol/sec. Considering the volume of water present in the well bore (approximately 33 gal, or 125 L), and the buffering capacity of bicarbonate offered by the native groundwater, approximately 6.5 x 10^{-3} mol/L, a significant period of time is required to achieve a substantial increase in pH (hence the results shown on Figure 5). Thus, a strategy involving flushing of the cathode well bore with aquifer water can substantially diminish the pH rise and hence reduce the calcite precipitation problem. The extracted water could then be treated and re-injected into the anode well bore. This strategy would offer the added benefits of preventing de-watering at the anode and would maintain electroosmotic water fluxes and Darcian flow in the same direction. For long-term operation, accumulation of calcite could be controlled relatively easily by temporarily shutting off the pumping system and reversing electrode polarity for short periods of time.

The capacity for a relatively modest pumping rate to control well bore pH was tested by applying a pumping rate of approximately 1 gal/min (3.9 L/min) to the pH test configuration described previously. pH was measured in W-1515, which was first used as a cathode and then converted to an anode by switching the polarity of the power supply. The resulting observed pH values are shown on Figures 6 and 7, respectively, along with pH values measured when pumping was not employed. In either the cathode or anode mode, pumping at this rate, corresponding to a flushing of one well bore volume approximately every 33 minutes, greatly reduced the electrolysis-induced pH effects. In contrast, the time-dependence of the electric current exhibited little difference between the pumped and non-pumped tests. This observation in part supports the assertion that calcite precipitation is perhaps not the principal explanation for the initial decline in electric current.

Measurement of Electroosmotic Flux

The heterogeneous nature of the local hydrogeology in the TFF area presented a number of challenges in conducting direct measurements of electroosmotic water fluxes induced by the application of a DC current. Although the electrode wells were all screened across primarily silty/clayey materials, thin sand fingers on the order of several inches in thickness were observed in soil cores and were also noted in interpretations of geophysical logs. As noted previously, pumping test results indicated that these sands were relatively permeable and served to connect the wells to one another hydraulically. Consequently, the expected de-watering of an anode well and the increase in hydraulic head at the cathode well resulting from electroosmosis would tend to be short-circuited as the resulting head gradients forced water to circulate back from the cathode(s) toward the anode(s) via Darcy's law. This phenomenon would render any direct measurement of water volumetric fluxes impractical. Similarly, a two-well tracer test for measuring travel time from the

anode well to the cathode well would suffer from the uncertainty associated with tracer migration through the permeable sand as a result of exclusively hydraulic effects.

In response to these challenges, a comparative single well tracer test plan was developed to measure the total electroosmotic flux across a well screen under a DC current (either at the anode well or the cathode well). This entailed placing a tracer within the well bore and measuring its rate of removal as a function of mixing and dilution; differences in the tracer concentration history between tests with the DC current both on and off would be indicative of the electroosmotic flux. A mechanical circulation system was devised to pump water from the well bore up to the surface and back again into the well (Figure 8). This system allowed simultaneous injection of the tracer at the base of the water column, at approximately 1 gal/min (3.9 L/min), while native groundwater was extracted at an equivalent rate from the top of the column, thus minimizing differences in hydraulic head between the well bore and the surrounding aquifer. This configuration also provided a convenient means of obtaining groundwater samples for analyses.

The well bore tracer test required the deployment of a tracer species which exhibited a number of favorable characteristics, including non-toxicity, resistance to electromigration, low volatility, and chemical stability under non-ambient conditions. For example, the potential for electromigration eliminated familiar ionic tracers such as bromide, while noble gas tracers such as helium or xenon were too volatile to be reliable. At the same time, the stability of fluorescent organic dyes, also commonly used as tracer compounds, was uncertain in the presence of the extreme redox and pH conditions encountered at the cathode and anode. The most suitable tracer identified for this test proved to be the water itself, labeled isotopically by its oxygen-18 fraction. The isotopic fractionation of oxygen in a water sample is usually given as a comparison between the $^{18}O/^{16}O$ ratios of the sample to that of standard mean ocean water (SMOW) and is referred to as $\delta^{18}O$. A negative value of $\delta^{18}O$ is indicative of water is depleted in the heavy oxygen-18 isotope relative to the SMOW, while a positive value indicates enrichment. Briefly, evaporation and condensation processes tend to fractionate the lighter ^{16}O –containing water molecules from those of the heavier ^{18}O- water. Water vapor generated by evaporation at colder temperatures tends to have strongly negative $\delta^{18}O$ values, with less negative values at higher temperatures. For this reason, differences in $\delta^{18}O$ between native groundwater in the TFF area, recharged locally, and tap water originating as Sierran snowmelt can be exploited to yield an effective tracer of well bore mixing. Specifically, the $\delta^{18}O$ values associated with native TFF groundwater, approximately –8.13, and tap water originating from the Hetch Hetchy Reservoir in Yosemite National Park, approximately -13.48, provided a broad dynamic range.

A total of four tests – two without an applied current and two with a 50 V difference between the electrodes in wells W-1514 and W-1515 – were conducted. Well W-1515 was utilized for the single well bore tracer test. The tests with the applied DC current involved different polaritities, so that the W-1515 electrode served as the anode for the first test and the cathode for the second. Each test lasted for approximately 3 days, with residual tracer extracted from the vicinity of the well bore by pumping out approximately 200 gallons (800 L, or roughly 6 pore volumes). The $\delta^{18}O$ values for the four tests as a function of time are shown on Figure 9; conversions of these data into the fraction of the tracer water present in the well bore are shown on Figure 10. The well bore tracer fraction data clearly indicate that much of the tracer, approximately half, is lost from the well bore at the start of each of the tests. Much of this loss may result from density differences between the tracer water and native groundwater. Groundwater in the TFF area remains at elevated temperature (35 to 40

C) several years after thermal treatment approaches (steam injection, electrical resistive heating) as a result of relatively slow rates of groundwater movement and the thermal insulating properties of the sediments. The tracer water, on the other hand, was held at the surface in a fiberglass bubble, exposed to temperatures only on the order of 25 to 30 C. Presumably, the colder and thus denser tracer water, injected at the base of the water column, tended to flow out of the well screen into the surrounding sand pack as well as into the sand fingers of the formation (Figure 11). This effect holds important implications for the interpretation of the tracer test results. When used as an anode, water will be generally drawn away from the vicinity of the well bore, which by itself exerts no immediate effect on the observed tracer concentration. However, the resulting decline in the hydraulic head within the well bore will cause water to flow back into the well by Darcy's law through the most permeable units, the sand fingers (Figure 11). The presence of tracer in these sand fingers implies the return of some of the tracer mass to the well bore, thus reducing the apparent rate of tracer loss in the well compared to the situation when no electrical current was applied. In the case of a cathode configuration in the well bore, water will be drawn toward the well from the formation, displacing tracer-laden water in the sand pack back into the well bore (Figure 11). The resulting increase in hydraulic head within the well will tend to drive the well bore water back out into the formation through the sand fingers, although this effect will not influence the tracer concentration in the well bore itself. Thus, with either electrode polarity, the tracer would be expected to remain longer within the well bore when a DC current is applied than when it is not.

The tracer data from the four tests are shown again on Figure 12, in this case normalized to the tracer concentration at the beginning of the monitoring period. This indicates how much of the well bore water has mixed with native groundwater following the initial tracer loss at the start of the test. The changes in well bore water fraction over time reflect several mechanisms, including natural groundwater advection (focused into the well by the relatively high permeability of the sand pack), along with dispersive mixing across the well screen, sand pack, and surrounding formation (enhanced by the re-circulating pumping action). Nevertheless, for measuring the electroosmotic flux, it is only the *differences* between the curves for the cases when electric current is applied, and when it is not, that are of interest. Therefore, for each of the two test pairs (first background test + W-1515 as an anode, second background test + W-1515 as a cathode), differences in well bore water fraction as a function of time were calculated. Specifically, for each sampling event from tests conducted with an applied electrical current, the difference between well bore water fraction and the corresponding well bore water fraction without the applied current were calculated. Mismatches in sampling times between the tests were addressed using linear interpolation between the sampling events when the electric field was not present. These differences, as a function of time, are shown for the two tests on Figures 13 and 14, respectively. For both tests, linear regression indicates a significant linear trend, with a slope of 0.002%/hr, corresponding to approximately 1.6 gal/day (6 L/day) given the 33 gallons (125 L) of water within the well bore. For comparison, a similar analysis of the differences between the two background test (i.e., the test where no current was applied) indicates no relationship (Figure 15). This result suggests that differences between the respective background and applied electric current tests are not likely to be merely the result of chance.

The estimated electroosmotic fluxes, taken with the electrode geometry, electric current, and bulk soil electrical conductivity can be used to estimate the bulk electroosmotic conductivity. The method used for this estimation is described later in this report (refer to "Modeling" section).

Long-Term System Performance

The long-term stability of the pH control strategy, as well as the sustainability of the electric current at constant voltage, are currently being assessed through a long-term operational test of the electroosmosis equipment installed in the TFF area. At the conclusion of the test, the results will be presented in an addendum to this report.

Modeling

Inverse Modeling of Bulk Electrical and Electroosmotic Conductivities

Bulk soil electrical conductivity, σ_s, for the electrode array at TFF was estimated using a semi-analytical solution to fit a best-estimate value of σ_s to the results of the four-electrode conductivity test described previously. The semi-analytical model utilizes a point source solution to the steady-state potential field problem, integrated in the vertical direction to simulate a line source (i.e., an electrode), to predict the potential (i.e., voltage) as a function of position with respect to the line source. Superposition allows for multiple electrodes, with the sign on the current flow through each electrode used to distinguish anodes and cathodes. Thus, the model accepts current flow as input and calculates the voltage difference across the electrodes. The model is based on a number of simplifying assumptions, most notably that the soil electrical conductivity is homogeneous and constant in time and that the three-dimensional model domain extends infinitely in all directions. The model also assumes that the line sources do not depart significantly from a vertical orientation, a reasonable assumption given the results of a vertical deviation survey of each of the four TFF electroosmosis wells that showed a departure of less than 2 feet over the entire depth range.

The construction of the semi-analytical model was performed using the MathCad (MathSoft, Inc.) computational environment (Attachment A). As illustrated, a bulk soil electrical conductivity of approximately 0.13 siemens/m reproduces the observed difference in voltage potential between the two passive wells, given the electrode geometry and measured electric current. The inferred voltage difference between the two active wells, approximately 23 V, is considerably less than the actual applied voltage (50 V). However, much of this apparent voltage loss can be explained by surface chemistry effects on the electrodes as well as by the resistance offered by the well bore water, PVC well casing, and sand pack. It is also possible that some of the difference may reflect heterogeneities in the soil electrical conductivity field in the vicinity of the electrodes. The effects of some of these potential heterogeneities were explored further using a numerical (finite-difference-based) modeling approach (Attachment B).

Because the electroosmotic velocity of water is, as an engineering approximation, proportional to the voltage gradient (Eq.-1), the semi-analytical model used to calculate the voltage potential distribution can easily be extended to calculate the local electroosmotic velocity field. That is, at any point in the model domain, the local groundwater velocity due strictly to electroosmosis is given by Eq.-1, with the electroosmotic conductivity, k_{eo}, as an input parameter and the voltage gradient calculated by numerical differentiation of the voltage potential line source model (Attachment C). Indeed, with a relationship in hand to quantify the flow field, the calculated summation of the electrosmotic fluxes across a cylindrical surface surrounding an electrode will provide an approximation to the flux of

water to the well (neglecting contributions across the top and the base of the cylinder). This calculation provides an opportunity to adjust the value of k_{eo} in the model so that the predicted flux matches that observed in field tests (i.e., the tracer test procedure described earlier). The resulting estimate for k_{eo}, roughly 2.3×10^{-9} m^2 sec^{-1} V^{-1}, is within the typical range reported for soils (1×10^{-9} to 10×10^{-9} m^2 sec^{-1} V^{-1}, Mitchell, 1993). Electroosmotic conductivity was directly measured in the laboratory by applying a voltage gradient across a single soil core from the W-1513 boring and measuring the resulting water flux. The k_{eo} was found to range between approximately $0.7 – 1.2 \times 10^{-9}$ m^2 sec^{-1} V^{-1} (N. Cherepy, personal communication, 1999).

Design Implications for Remediation Scale Deployment

The semi-analytical model described above can readily be extended to forecast system performance in terms of remediation, assuming that the calibrated parameters estimated in the TFF tests may be applied to other areas at the LLNL Livermore Site. In particular, particle tracking may be employed to calculate travel time from a point within the electrode array to the nearest cathode well under electroosmotic migration. This travel time may then be compared to a similar calculation involving hydraulic pumping in fine-grained material.

Calculated travel time in a 15 ft by 15 ft. (4.6 m by 4.6 m) four-electrode array, with 15 amps per electrode pair, is calculated in the MathCad model given in Attachment D. These calculations assume parameter values from the TFF tests (σ_s of 0.13 S/m, and k_{eo} of 2.3×10^{-9} m^2 sec^{-1} V^{-1}). The result is approximately 5.3 years of operation to draw a contaminant from the center of the array to one of the cathodes, at approximately 1 kW of power per electrode pair (67 V difference). However, because of the voltage drop across the well bore as discussed previously, the actual voltage drop, and hence power, would probably be larger (i.e., roughly twice the model results, or 2 kW per pair with a 140 V difference).

For comparison, an analogous calculation was performed to assess the rate at which hydraulic pumping could transport a contaminant from the same origin to an extraction well functioning at the cathode location (Attachment E). For this calculation, Darcy's law is substituted for Ohm's law, so that electric current is replaced by water flux, voltage potential by hydraulic head, and electrical conductivity by hydraulic conductivity. Hence, each cathode or anode well becomes a hydraulic injection or extraction well, respectively. The model assumed a hydraulic conductivity of 1×10^{-8} cm/s (matching that measured for fine-grained soils in the W-1513 core from TFF) and an optimistic head difference between the extraction and injection wells of approximately 120 ft (37 m) (i.e., 60 ft (18.3 m) of head buildup in the injection well and 60 feet (18.3 m) of drawdown in the extraction well). Under these assumptions, the flow rate to the extraction wells is only on the order of 1×10^{-4} gal/min (3.9×10^{-4} L/min). This implies a particle travel time from the array center to an extraction well of approximately 227 years, clearly far longer than that required for electroosmotically-driven transport.

Conclusions

The overall goal of this Qualification Phase testing effort for electroosmosis has been to ascertain the suitability of the technology for application to groundwater cleanup at the LLNL Livermore Site. The specific findings of the tests lend support to the notion of deploying this technology:

- A strategy for controlling pH in the electrode well bores, based on pumping of ambient groundwater, has been developed and demonstrated.
- A novel single well bore tracer test technique has been developed for estimating the electroosmotic flux to a well that is independent of laboratory bench-top techniques used on small cores.
- Estimates for the bulk soil electrical conductivity and bulk soil electroosmotic conductivity have been developed that are consistent with the ranges of values reported in the literature and are also consistent with values developed from independent laboratory tests on soil cores collected from the test area.
- A semi-analytical model for simulating electroosmotic fluxes in association with line source electrodes has been developed, validated, and calibrated. Application of the model to a deployment scale electrode configuration and electric current suggests that cleanup times in fine-grained soils (i.e., hydraulic conductivity ~ 1 x 10^{-8} cm/s, as measured in test area soil cores) are faster than those achievable by hydraulic pumping alone by a factor of approximately 40.

In summary, the findings of the Qualification Phase tests all point to the conclusion that electroosmosis can significantly improve the cleanup of fine-grained source areas at the LLNL Main Site and thus that the technology should be advanced to the Deployment Phase.

References

Acar, Y.B., and A.N. Alshawabkeh, Principles of Electrokinetic Remediation, *Environmental Science and Technology*, 27(13), 2638-2647, 1993.

Athmer, C.J., S.V. Ho, B.M. Hughes, P.W. Sheridan, P.H. Brodsky, and others, *Development of an Integrated in situ Remediation Technology, Draft Topical Report*, Monsanto Corporation, 1997.

Bruell, C.J., Segall, B.A., and M.T. Walsh, Electroosmotic removal of gasoline hydrocarbons and TCE from clay, *Journal of Environmental Engineering*, 118(1), 68-83, 1992.

Casagrande, I., Review of past and current work on electroosmotic stabilization of soils, *Harvard Soil Mechanics Series 38, Supplement 1957*, 1952.

Hamed, J., Acar, Y.B., and R.J. Gale, Pb(II) removal from kaolinite by electrokinetics, *Journal of Geotechnical Engineering*, 117(2), 241-271, 1991.

Happel, A.M., R.W. Bainer, L.L. Berg, M.D. Dresen, and A.L. Lamarre (Eds.), *Application for Containment Zone for the Livermore Site Hydrocarbon Impacted Zone at Treatment Facility F*, Lawrence Livermore National Laboratory, UCRL-AR-123385, July, 1996.

Jacobs, R.A., and Probstein, R.F., Two-dimensional modeling of electroremediation, *AICHE Journal*, 42(6), 1685-1696, 1996.

Lageman, R., Electroreclamation, *Environmental Science and Technology*, 27(13), 2648-2650, 1993.

Mitchell, J.K., Fundamentals of Soil Behavior, 2nd Edition, John Wiley and Sons, New York, New York, 437 p., 1993.

Pamukcu, S., and M. Pervizpour, *Electroosmotically Aided Restoration of TCE Contaminated Soil, Department of Civil and Environmental Engineering, Final Report to Lawrence Livermore National Laboratory*, Lehigh University, 1998.

Parkhurst, D.L., *User's guide to PHREEQC – A Computer Program for Speciation, Reaction-path, Advective-transport, and Inverse Geochemical Calculations*, U.S. Geological Survey Water Resources Investigation Report 95-4227, Lakewood, Colorado, 143 p., 1995.

Probstein, R.F., R.E. Hicks, Removal of contaminants from soils by electric fields, *Science*, 260(5107), 498-503, 1993.

Segall, B.A., and C.J. Bruell, Electroosmotic contaminant removal processes, *Journal of Environmental Engineering*, 84-100, 118(1), 1992.

Shapiro, A.P., R.F. Probstein, Removal of contaminants from saturated clay by electroosmosis,*Environmental Science and Technology*, 27(2), 283-291, 1993.

Table 1A. Soil concentrations in W-1115 at a depth of 118 ft (July, 1995).

Hydrocarbon	**Conc. (mg/Kg)**
TPH-g	8,600
Xylenes (total)	942
Toluene	397
Ethylbenzene	168
Benzene	8.6

Table 1B. Groundwater concentrations of fuel hydrocarbons in W-1115 (July, 1995).

Hydrocarbon	**Conc. (μg/L)**
TPH-g	61,400
m-,*p*-Xylenes	7,590
Toluene	5,700
o-Xylene	5,160
1,2,4-Trimethylbenzene	3,840
Ethylbenzene	3,140
Benzene	2,350
1,2,3-Trimethylbenzene	1,390
n-Propylbenzene	610
1,3,5-Trimethylbenzene	240
i-Propylbenzene	230

Table 2. Hydraulic Test Analysis for W-1514
Observation Wells 1513 and 1515

Modified Nonequilibrium Equation (semi-log or Cooper-Jacob)
Driscoll (1986) page 221 equations 9.7 and 9.8

		Early				Late	
Well		T (gpd/ft)	K (gpd/ft^2)	S	Ss	T (gpd/ft)	K (gpd/ft^2)
W-1513	Observation	612	87	0.003	0.0004	2355	336
W-1514	Pumping	450	90	0.31	0.06	1020	204
W-1515	Observation	729	145	0.0032	0.0006	2552	510

Water-level recovery data
Driscoll (1986) page 256 equation 9.16

Well		T (gpd/ft)	K (gpd/ft^2)
W-1513	Observation	502	72
W-1514	Pumping	356	71
W-1515	Observation	638	127

Theis Confined

Well		T (gpd/ft)	K (gpd/ft^2)	S	Ss
W-1513	Observation	393	56	0.003881	0.0006
W-1514	Pumping	440	88	0.4304	0.086
W-1515	Observation	502	100	0.004456	9.20E-05

Leaky-Hantush

Well		T (gpd/ft)	K (gpd/ft^2)	S	Ss
W-1513	Observation	1069	153	0.00011	0.000015
W-1514	Pumping	533	106	0.04693	0.009
W-1515	Observation	1462	292	0.000092	1.80E-05

Table 3. TFF EO Resistivity Tests

Time (min)	VDC	DC Amps	Polarity (1513)	Polarity (1515)	VDC (diff. b/w 1514 and 1115)	+0.683 VDC offset)
1	10.2	0.9	+	-	0.791	0.108
2	10.2	0.9	+	-	0.792	0.109
3	10.2	0.9	+	-	0.792	0.109
5	10.2	0.9	+	-	0.792	0.109
1	10.02	1	-	+	0.569	-0.114
2	10.04	0.9	-	+	0.575	-0.108
3	10.01	0.8	-	+	0.58	-0.103
5	10.08	0.8	-	+	0.584	-0.099
1	20	2	+	-	0.93	0.247
2	20.03	2.1	+	-	0.914	0.231
3	20.05	2.1	+	-	0.914	0.231
4	20.03	2.1	+	-	0.915	0.232
5	20.03	2.1	+	-	0.915	0.232
1	20.03	2	-	+	0.458	-0.225
2	20.06	1.9	-	+	0.465	-0.218
3	20.07	1.8	-	+	0.467	-0.216
4	20.08	1.8	-	+	0.467	-0.216
5	20.08	1.8	-	+	0.467	-0.216
1	30.01	3.4	+	-	1.035	0.352
3	30.03	3.4	+	-	1.036	0.353
1	30.04	3.1	-	+	0.343	-0.34
4	30.4	2.9	-	+	0.343	-0.34
1	40	4.6	+	-	1.158	0.475
4	40	4.6	+	-	1.158	0.475
1	40.06	4.1	-	+	0.23	-0.453
4	40.09	3.9	-	+	0.232	-0.451
1	50.03	5.6	+	-	1.281	0.598
4	50.03	5.6	+	-	1.281	0.598
1	50.05	5.5	-	+	0.116	-0.567
4	50.06	5.4	-	+	0.114	-0.569

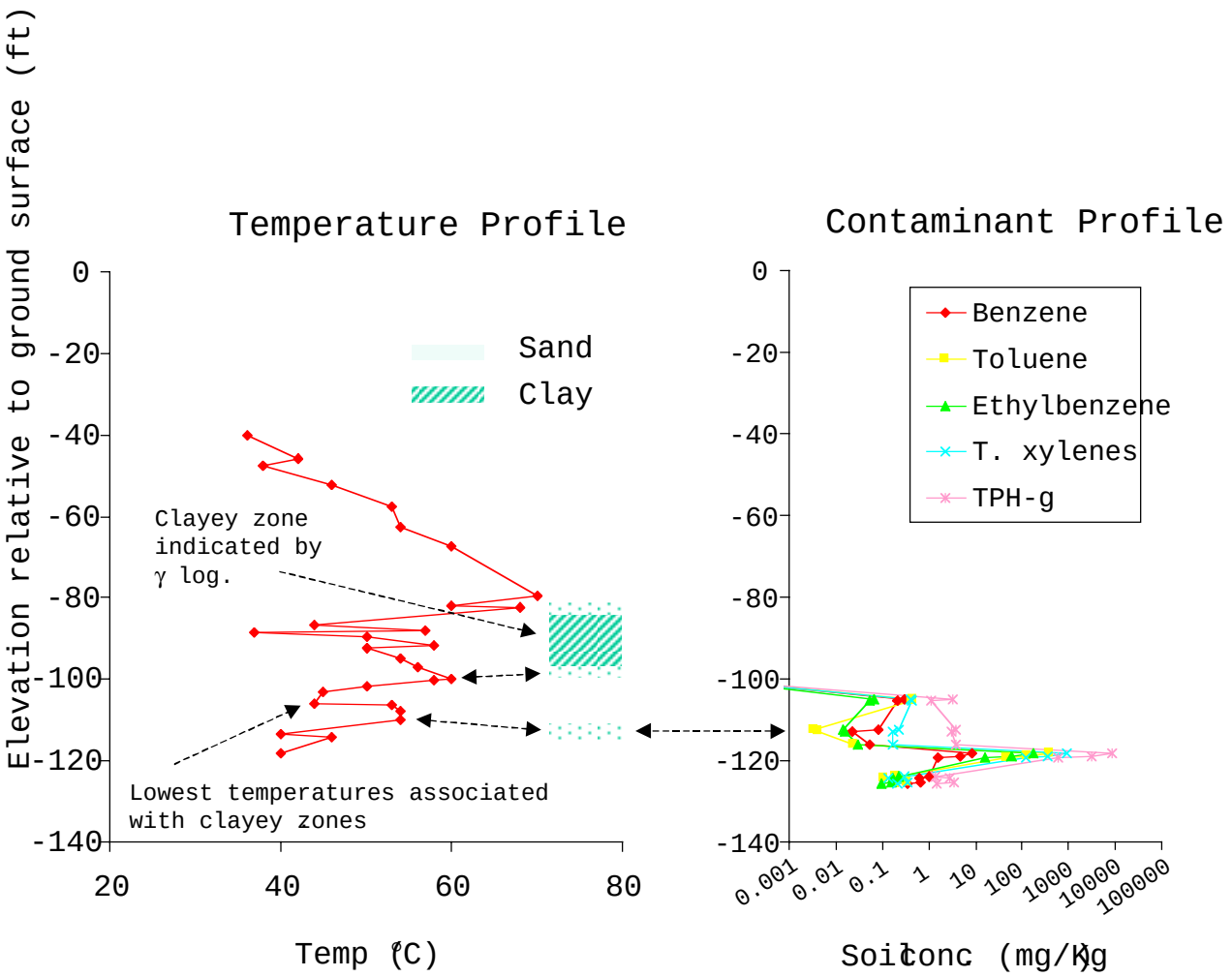

Figure 1. Lithology of W-1115 in the TFF area, indicating the relationships between temperature, lithology, and hydrocarbon concentrations in soil (1995 data).

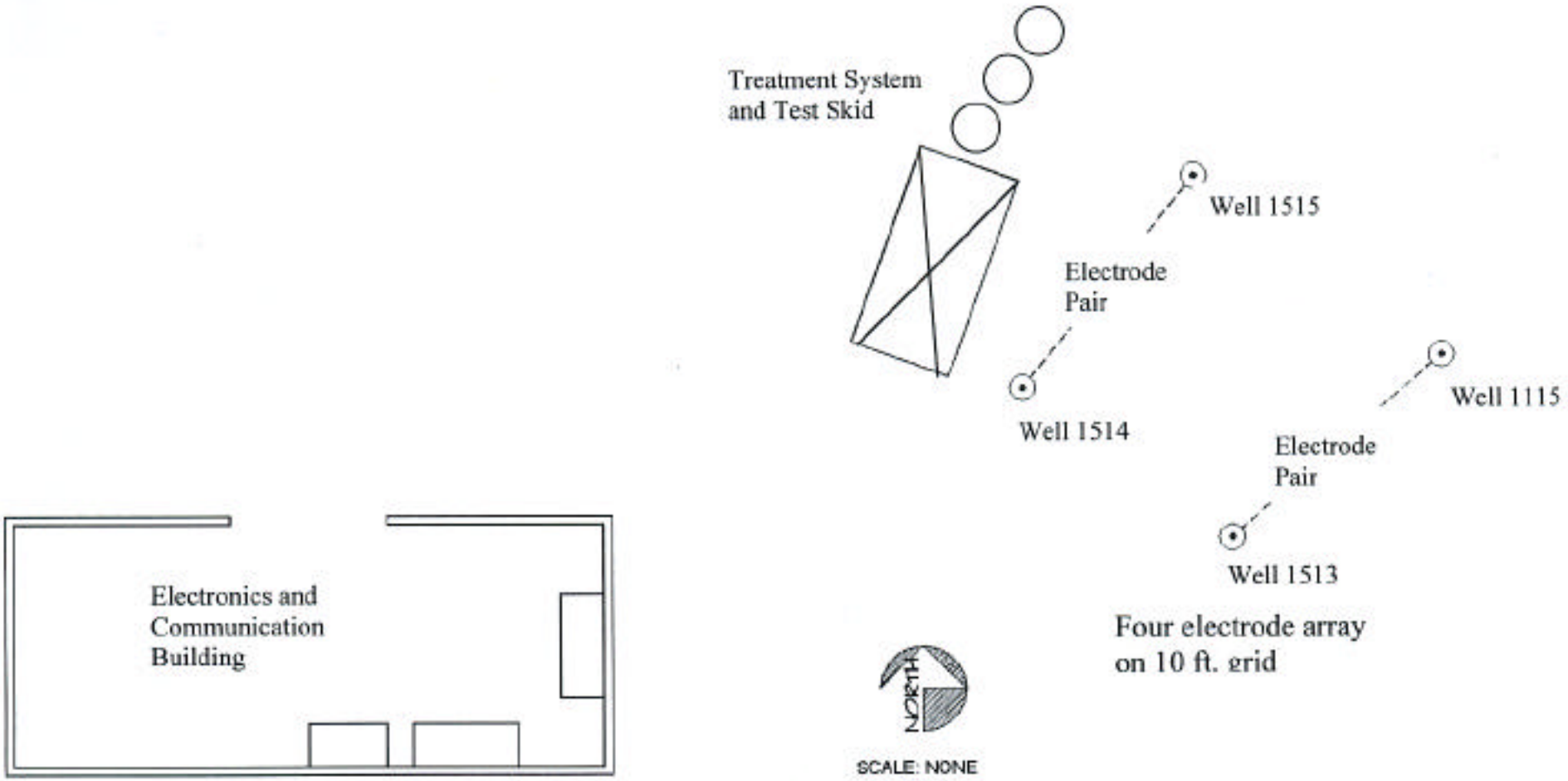

Figure 2. Arrangement of groundwater wells in the TFF area used to house the electrode array for the Qualification Phase testing.

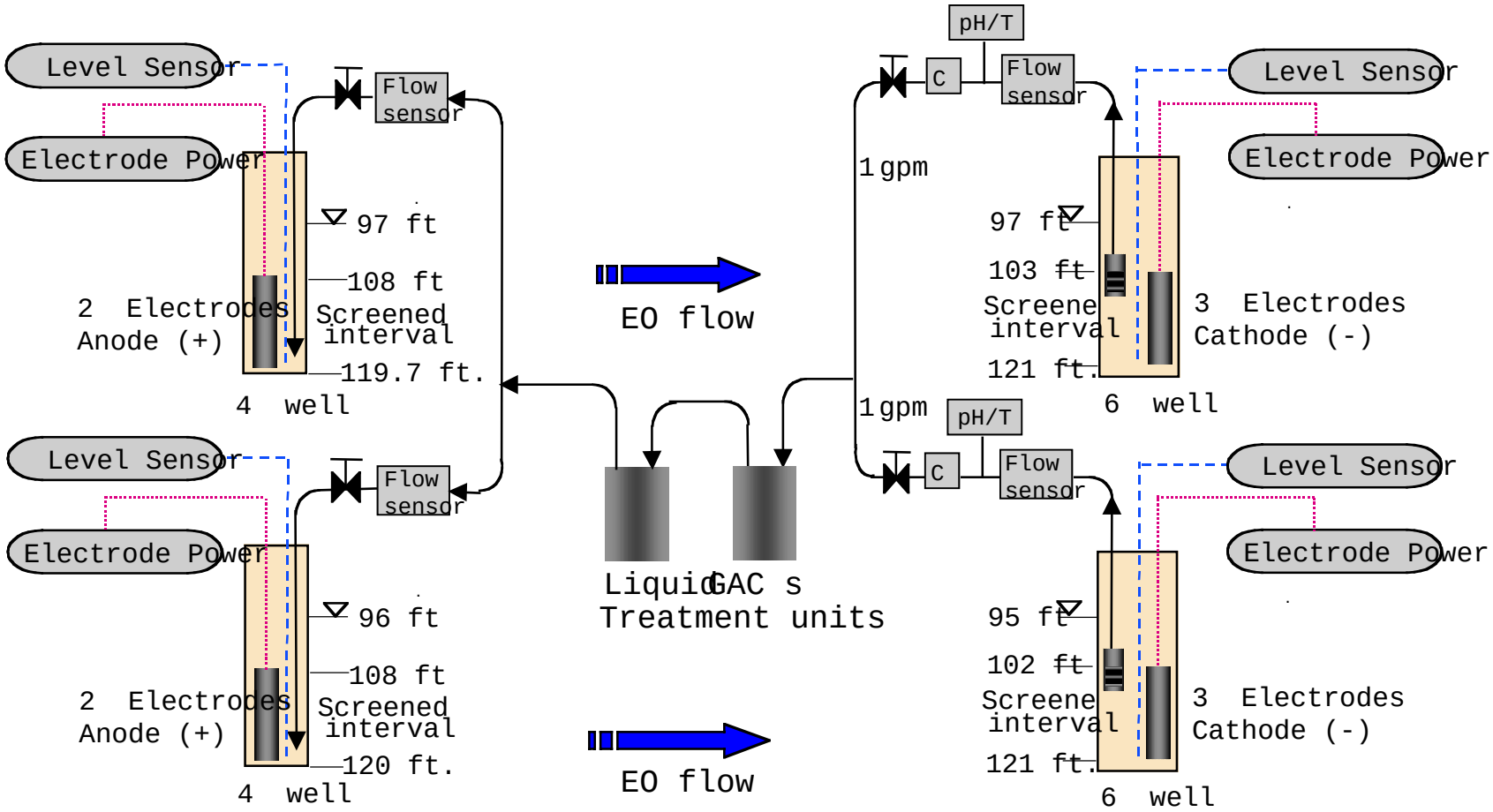

Figure 3. Schematic depiction of the equipment supporting the electroosmosis tests.

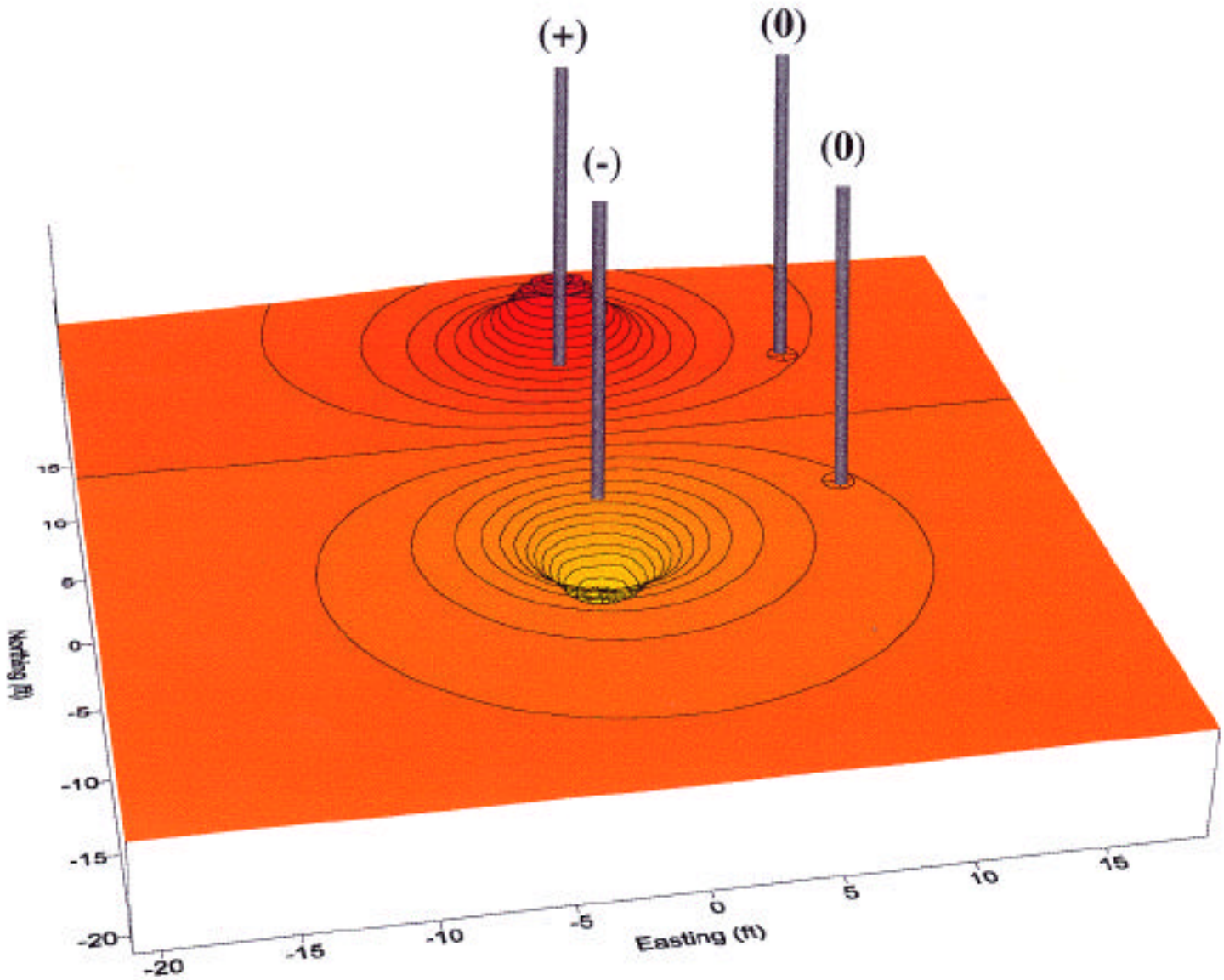

Figure 4. Hypothetical voltage potential distribution associated with a four-electrode resistivity test.

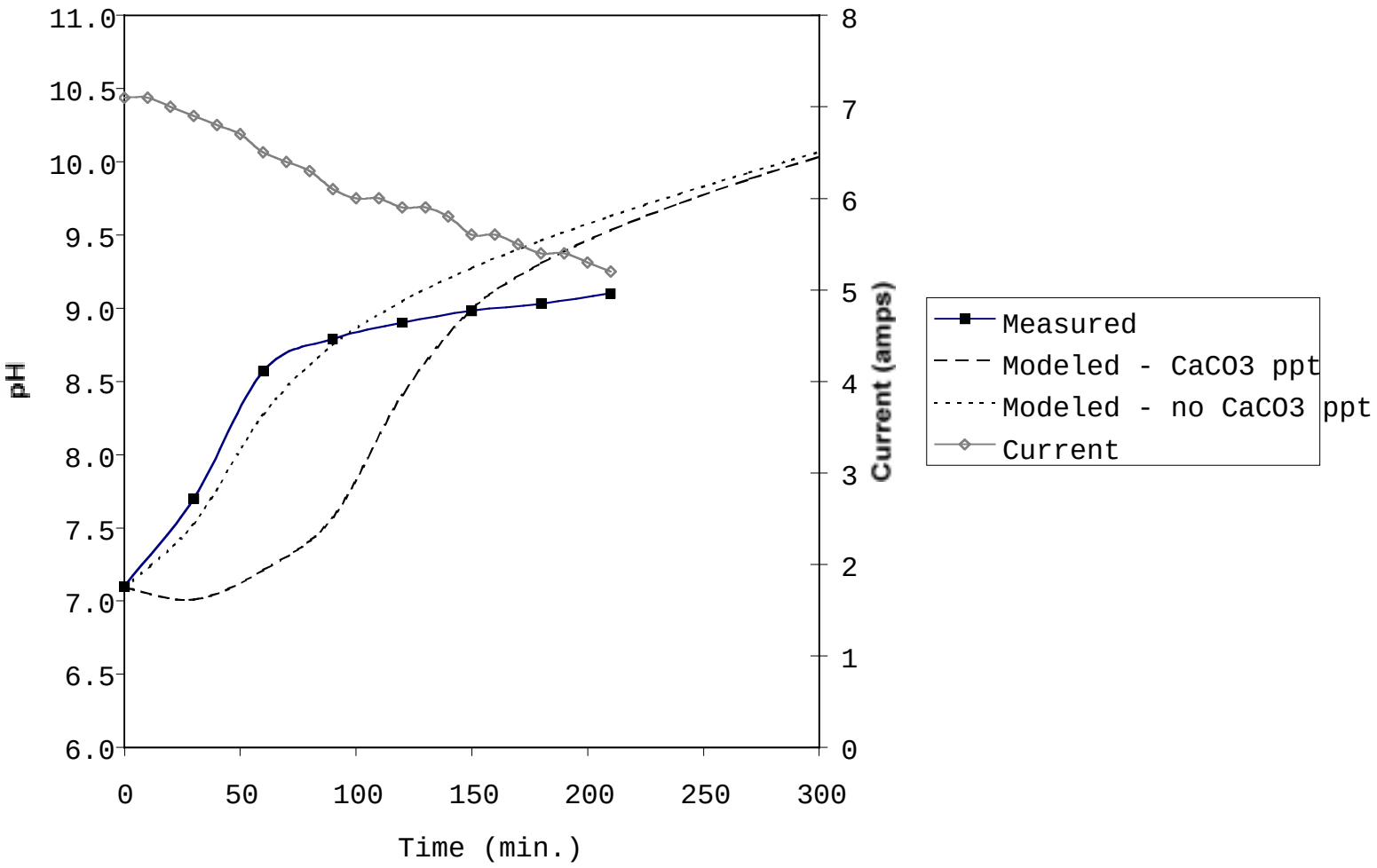

Figure 5. pH response to hydroxide loading and calcite precipitation at the cathode well: observed and simulated.

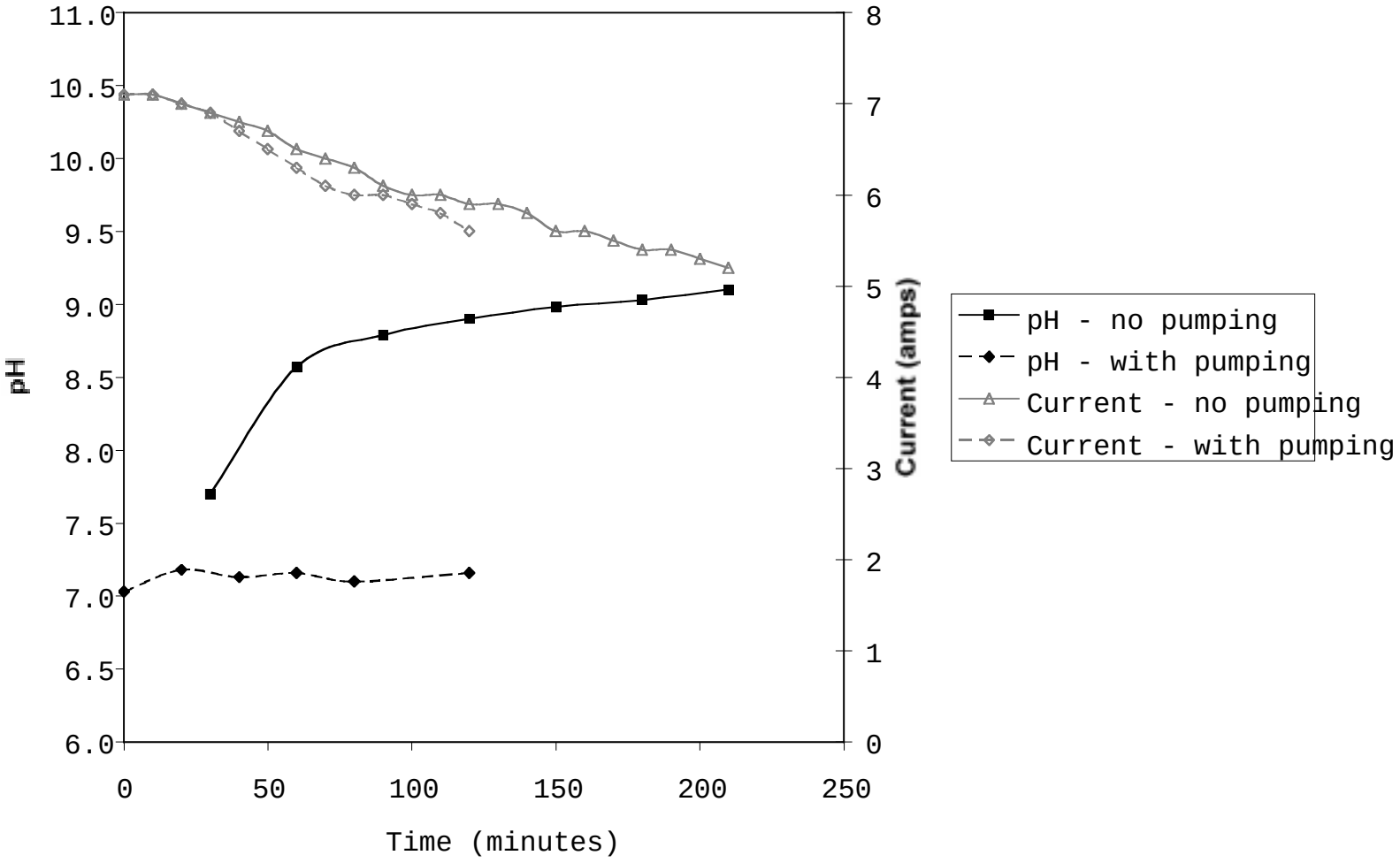

Figure 6. pH response over time in the cathode well (pumped and un-pumped).

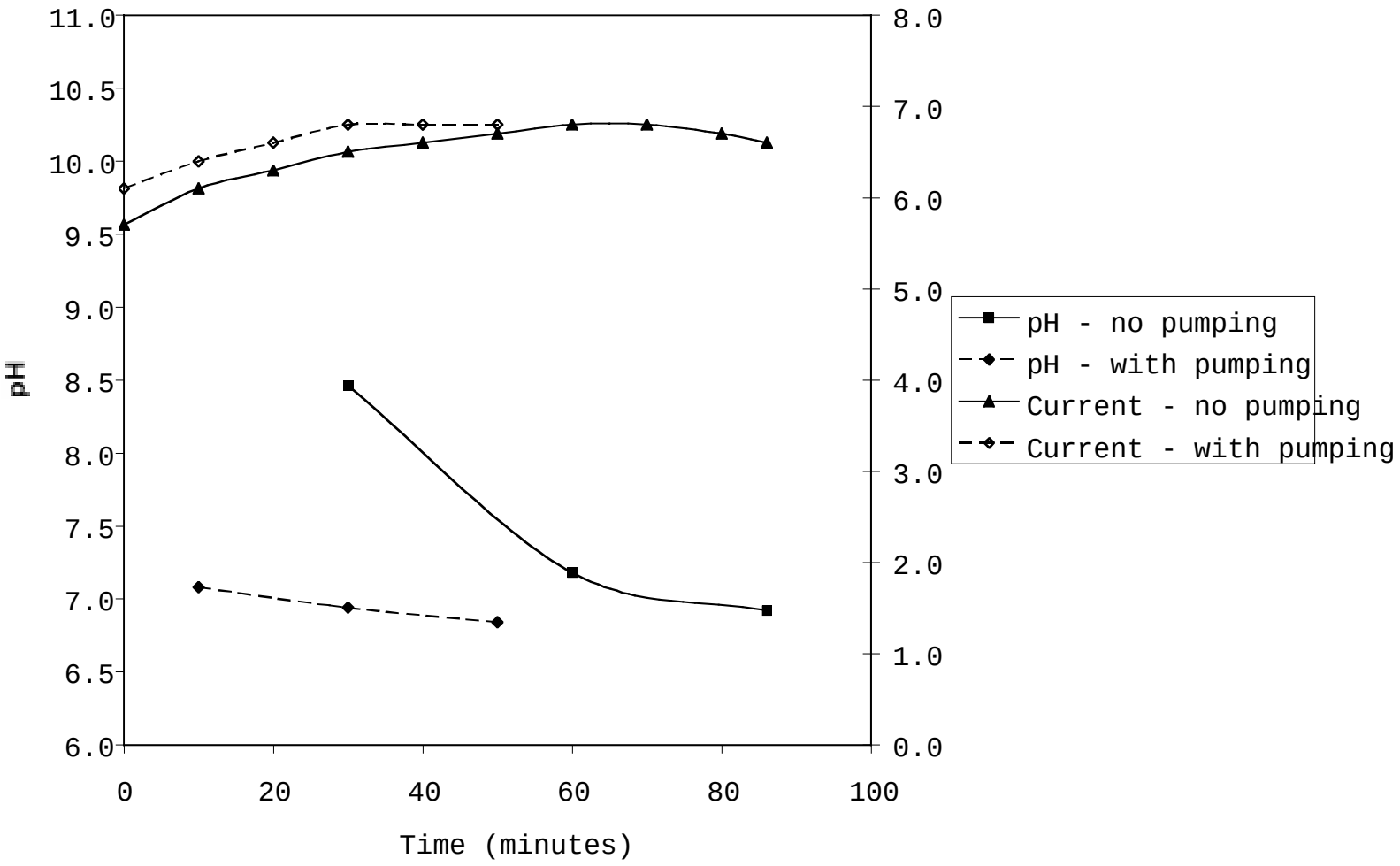

Figure 7. pH response over time in the anode well following polarity switching (pumped and un-pumped).

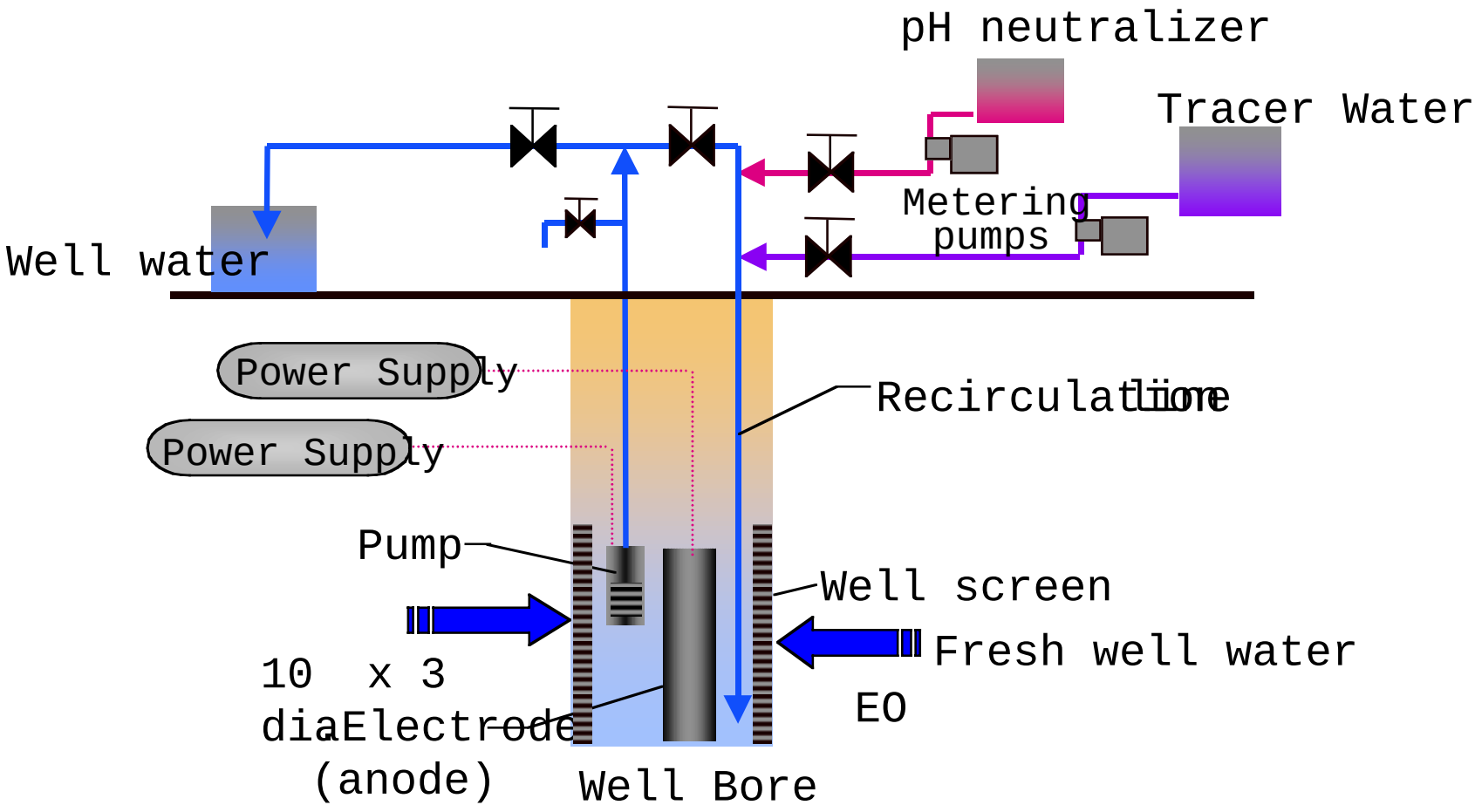

Figure 8. Re-circulating well configuration for tracer tests.

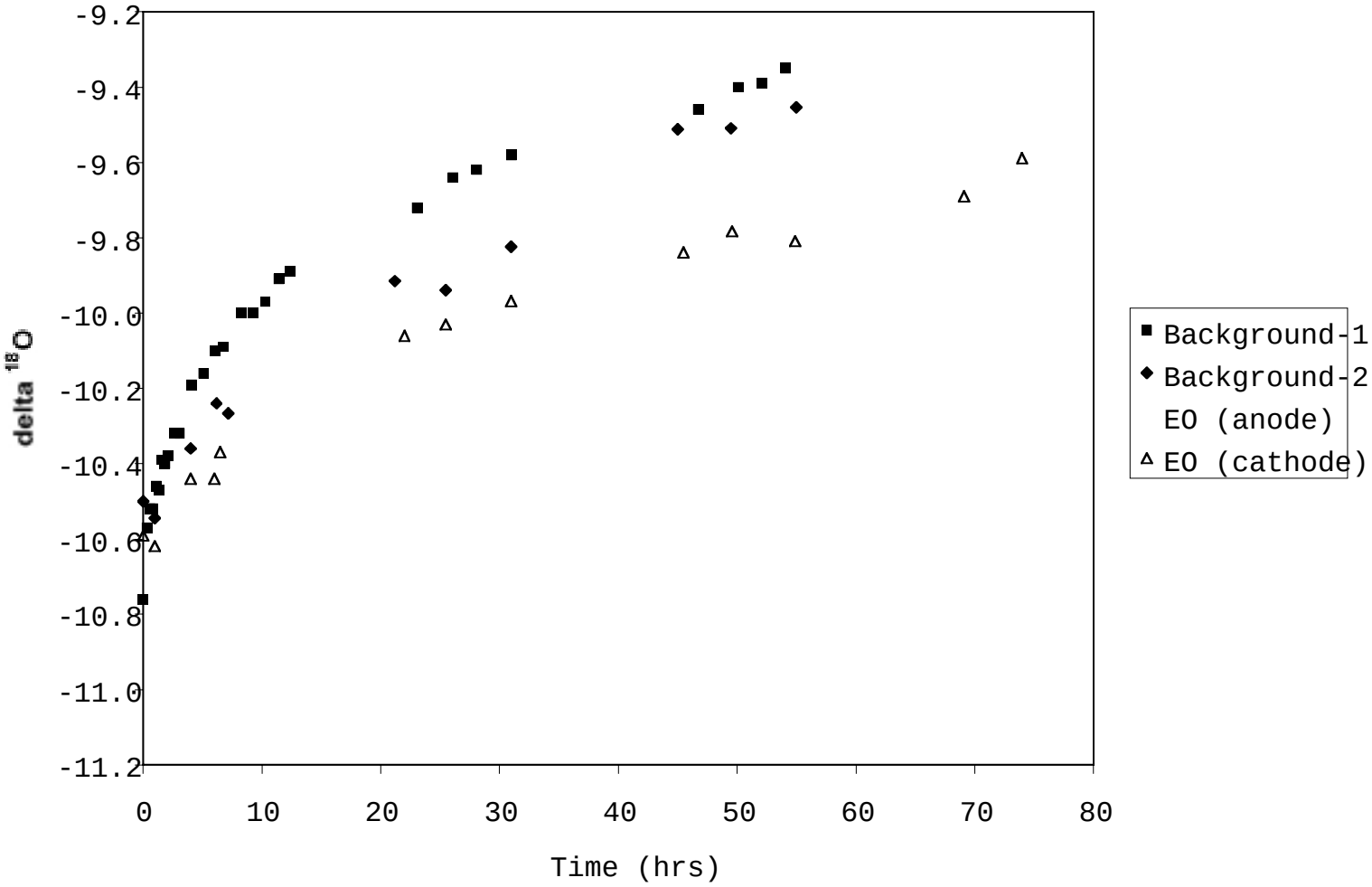

Figure 9. $\delta^{18}O$ measurements in W-1515 during each of the tracer tests (background and with applied electric field) as a function of time.

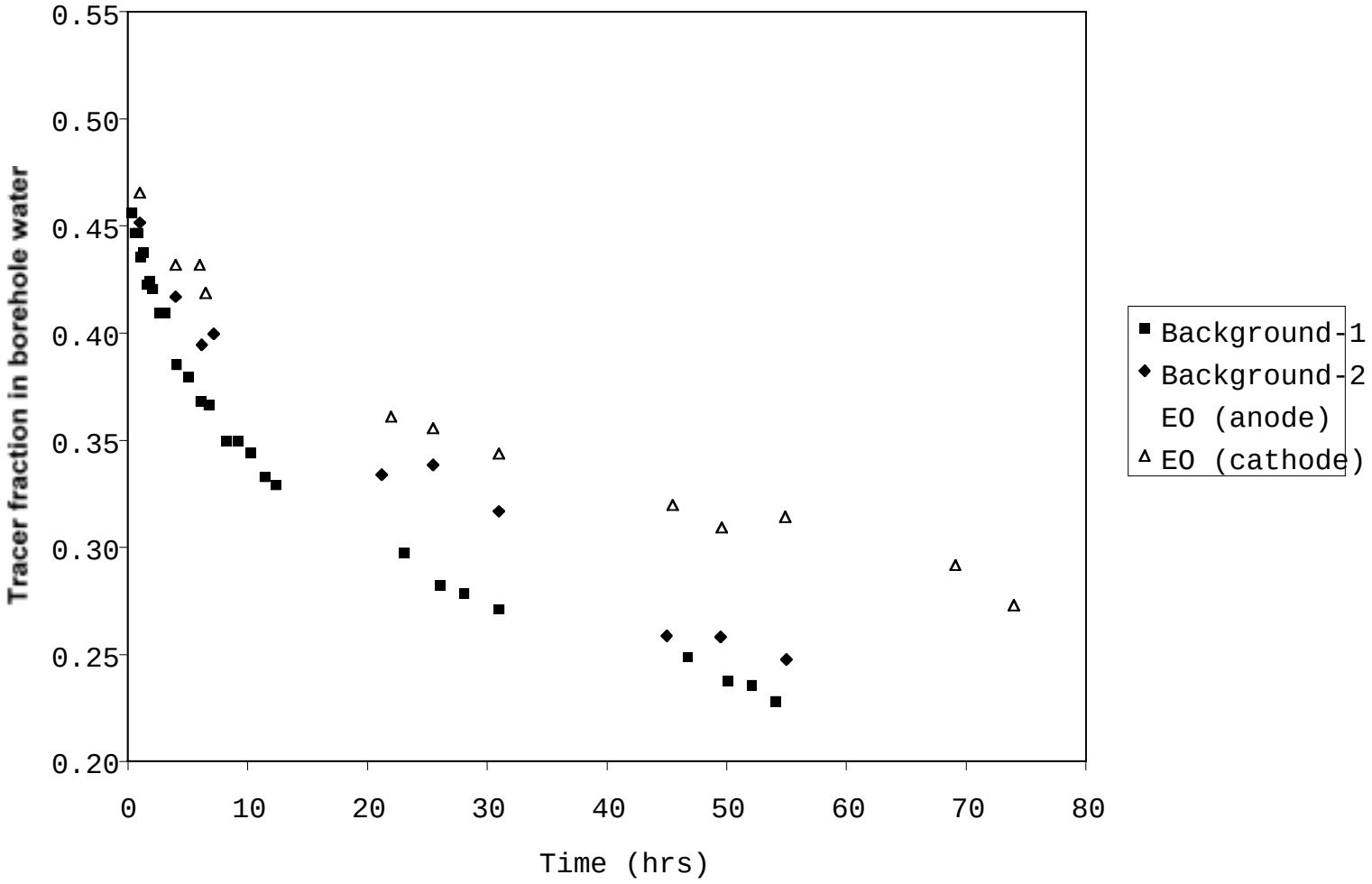

Figure 10. Tracer test results, with $\delta^{18}O$ measurements converted to the fraction of the original tracer (Hetch Hetchy tap water) present in the well bore over time.

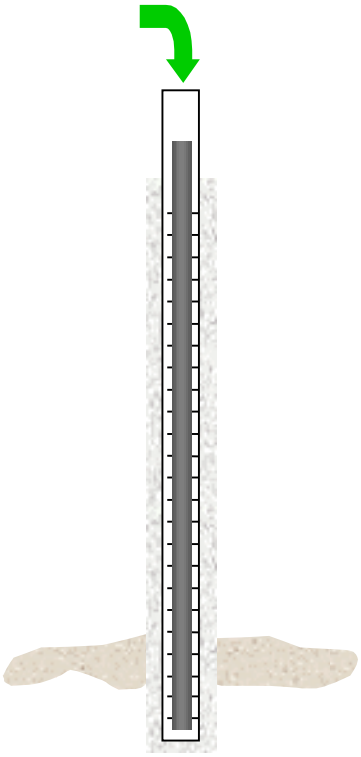

1. Tracer is injected into well while native bore hole water is removed simultaneously.

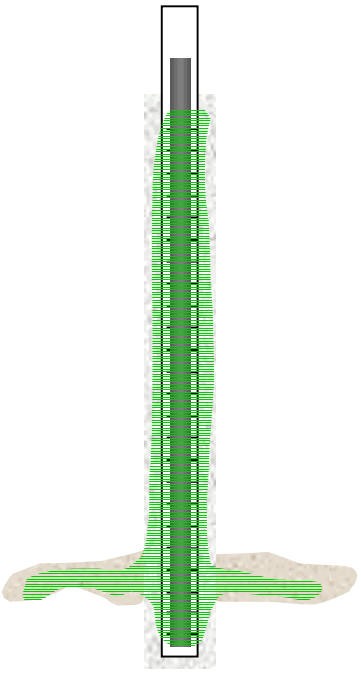

2. Density differences due to temperature differences force tracer out into sand pack and adjacent formation sands. Effects of background (i.e. no EO) advection and mixing on tracer concentration measured. Recirculation pump used to keep tracer well-mixed.

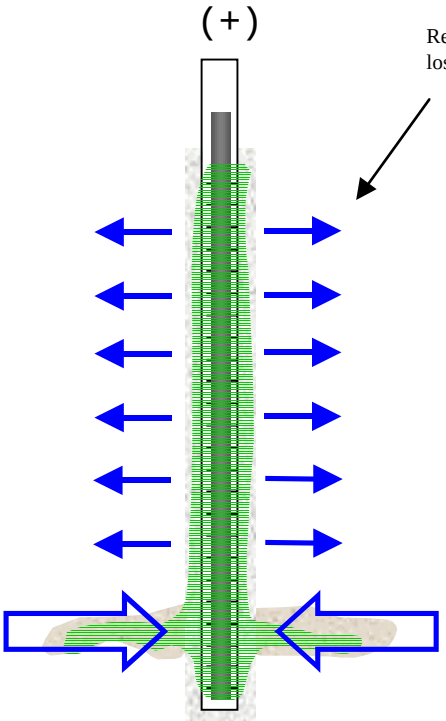

Regardless of polarity, EO retards the initial loss of tracer from the borehole.

3. As an anode well, bore hole water is drawn away from the well into the clay (no net concentration change). However, tracer-laden water moves back into well from formation sands because of induced head gradient.

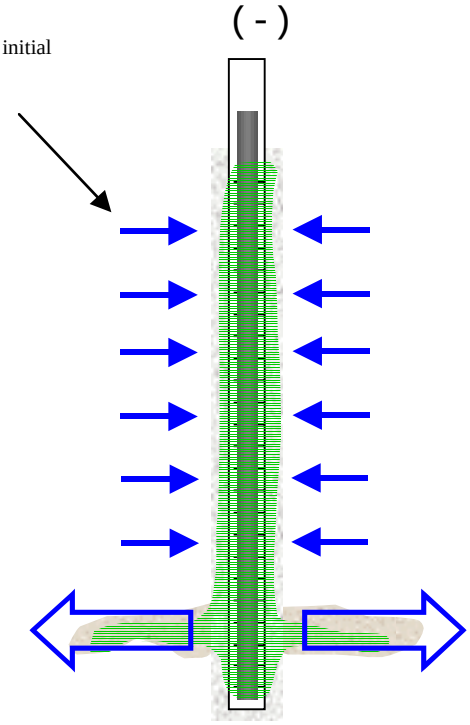

4. As a cathode well, formation water is drawn toward well, carrying tracer back into bore hole from sand pack. Darcy's law-induced outflow into formation sand does not affect tracer concentration in bore hole.

Figure 11. Scenarios of tracer movement during the tracer tests conducted in W-1515.

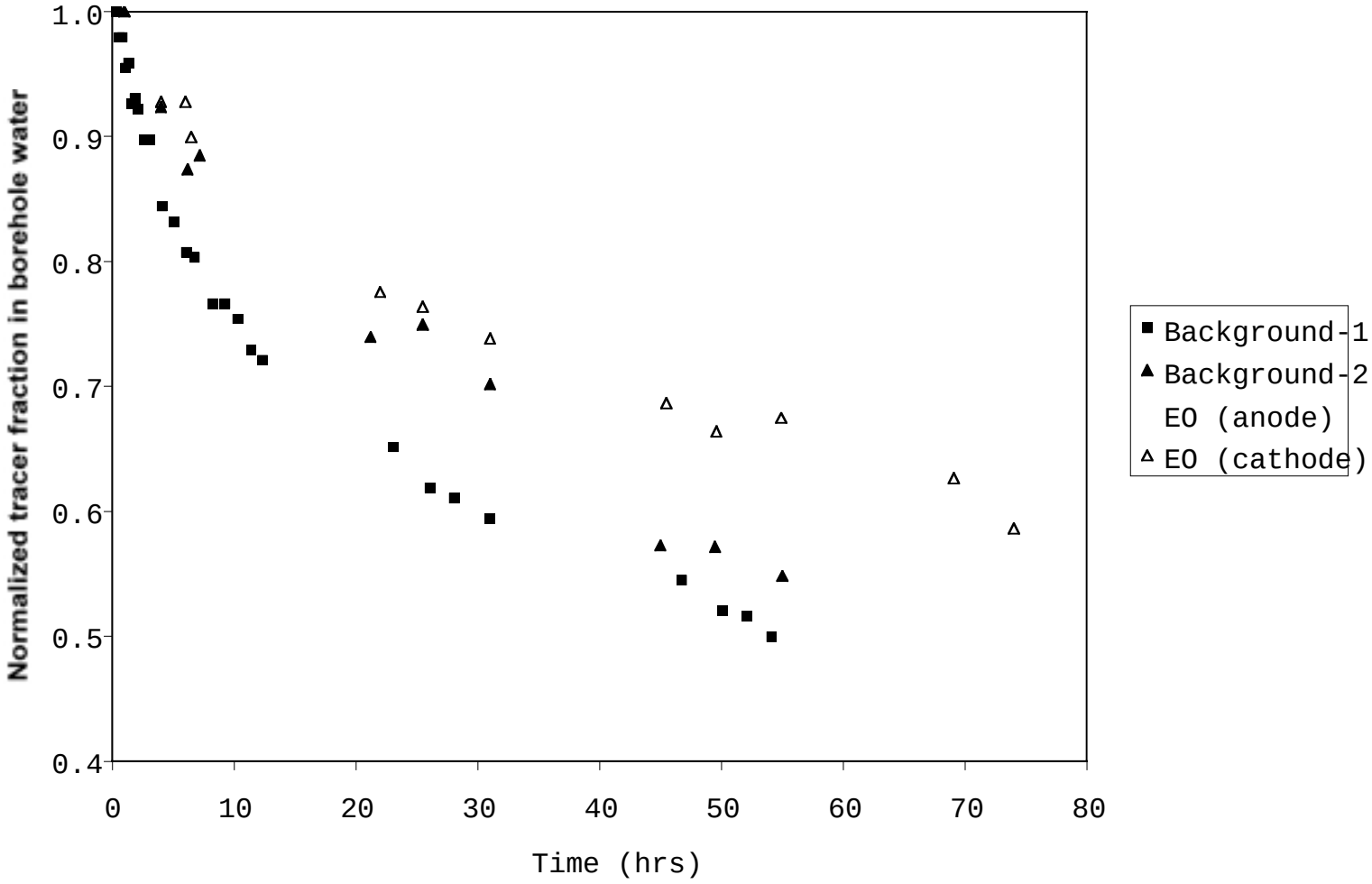

Figure 12. Tracer fraction in the well bore over time, normalized to the fraction at the beginning of the monitoring period.

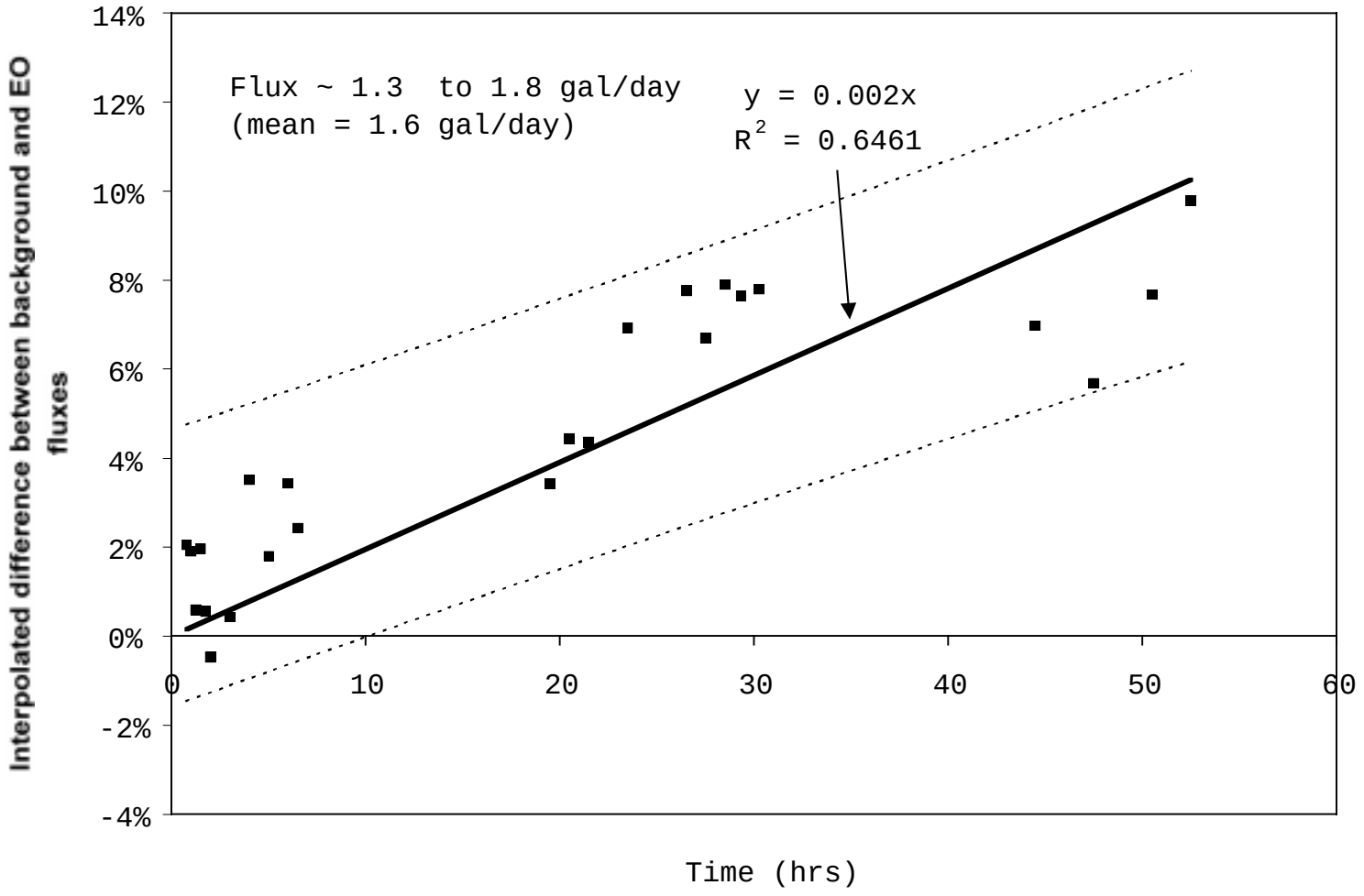

Figure 13. Differences in normalized well bore tracer fraction between the background test (no electric current) and a voltage difference of 50 V, with W-1515 housing the anode. Dashed lines show 95% prediction bands.

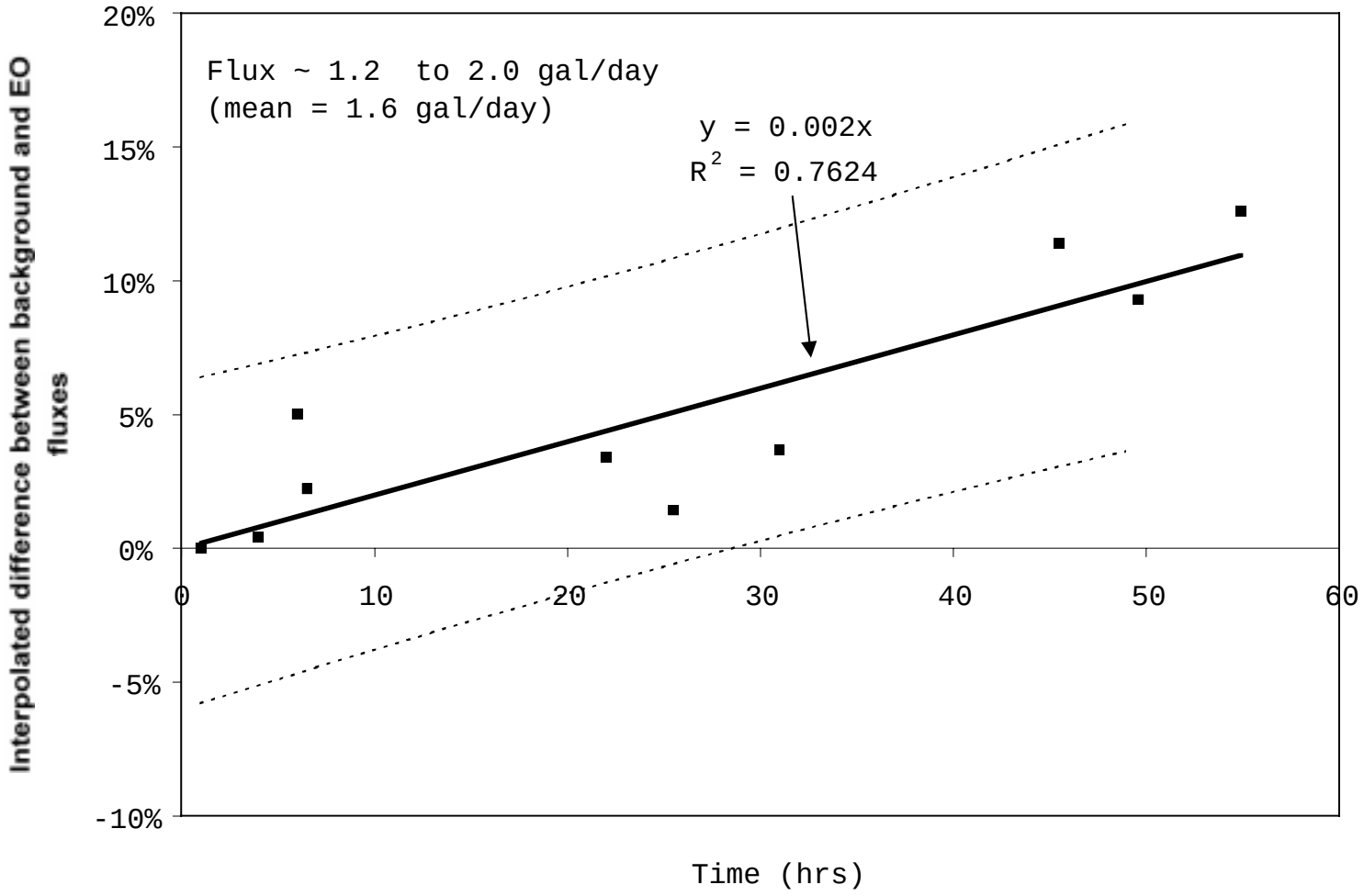

Figure 14. Differences in normalized well bore tracer fraction between the background test (no electric current) and a voltage difference of 50 V, with W-1515 housing the cathode. Dashed lines show 95% prediction bands.

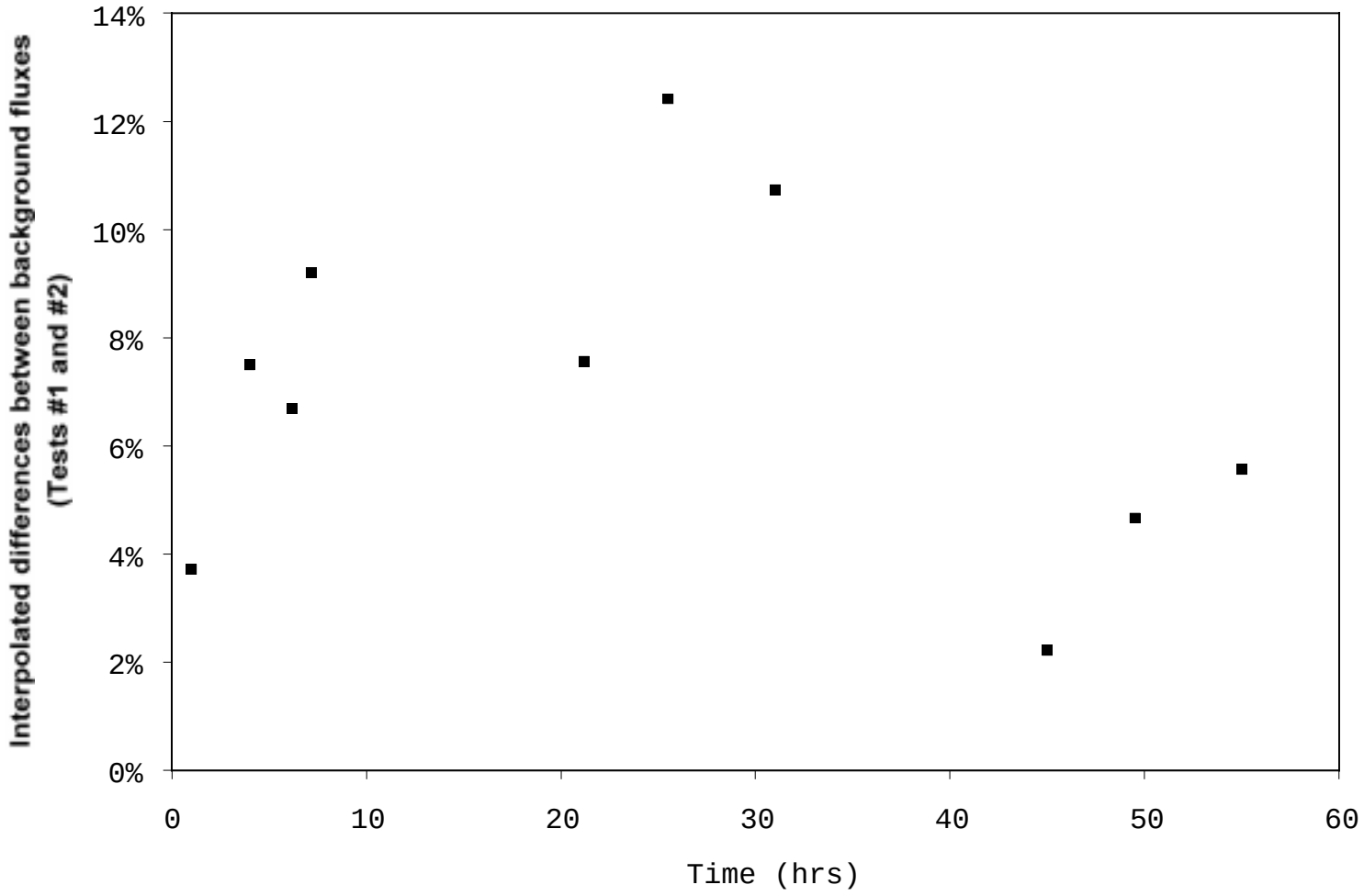

Figure 15. Differences in normalized well bore tracer fraction between the two background tests, indicating no discernible trend.

Attachment A

Semi-Analytical Model for Voltage Distribution from Line Sources of Electric Current in an Infinite, Homogenous Three-Dimensional Domain

Bulk Electrical Conductivity Screening Model

This 3-D model is based upon the assumption that the electric field may be defined using simple potential theory. Cathodes and anodes are modeled as electron sources and sinks, respectively, using a continuous point source solution in an infinite homogeneous 3-D domain. Point sources are then integrated in the vertical direction to simulate a continuous line source (i.e. finite electrode).

Sediment Properties

$\sigma_S := 0.128 \frac{S}{m}$ (electric conductivity - based on best fit to 4-electrode resistivity test)

EO System Properties

$E_L := 10ft$ (electrode length)

$E_d := 3in \quad r_e := \frac{E_d}{2}$ (electrode diameter and radius)

$E_A := \pi \cdot r_e \cdot (2 \cdot E_L + r_e)$ (electrode surface area)

Electrode configuration (elevation with reference to bottom of electrode):

$N := 4$ (total number of electrodes)

$ORIGIN \equiv 1$ (set first array index = 1)

Geometrical arrangement of electrodes is based on a regular grid, constrained by the given spacings in the x- and y-directions.

$$c_e := \begin{bmatrix} 0.0 \\ 0.0 \\ -120 \end{bmatrix} ft$$ (location of reference cathode)

$\Delta x := 10ft$ (east-west spacing) $\Delta y := 10ft$ (north-south spacing)

$$x_e := \begin{bmatrix} c_{e_1} \\ c_{e_1} + \Delta x \\ c_{e_1} \\ c_{e_1} + \Delta x \end{bmatrix} \quad y_e := \begin{bmatrix} c_{e_2} \\ c_{e_2} \\ c_{e_2} + \Delta y \\ c_{e_2} + \Delta y \end{bmatrix} \quad z_e := \begin{bmatrix} c_{e_3} \\ c_{e_3} \\ c_{e_3} \\ c_{e_3} \end{bmatrix} \quad I := \begin{bmatrix} 5.4 \\ 0.0 \\ -5.4 \\ 0.0 \end{bmatrix} amp$$

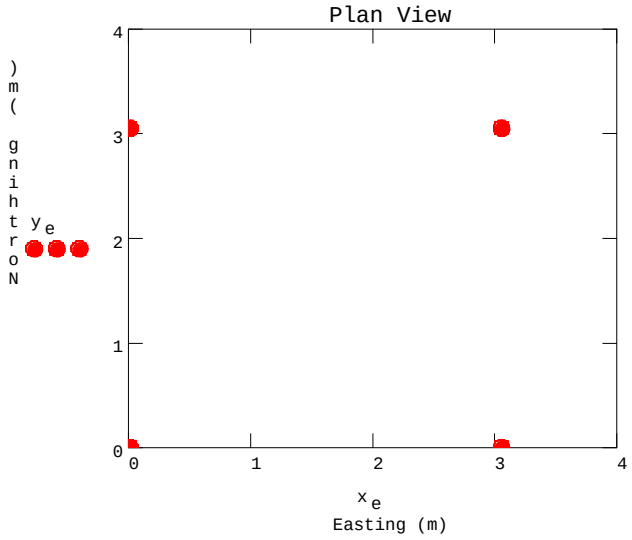

Potential Field Equations

Distance equation in 3-D:

$$dist3(x_1, y_1, z_1, x_2, y_2, z_2) := \sqrt{(x_1 - x_2)^2 + (y_1 - y_2)^2 + (z_1 - z_2)^2}$$

Potential distribution:

$$\phi(x, y, z) := \sum_{k=1}^{N} \frac{1}{E_L} \cdot \int_{z_{e_k}}^{z_{e_k} + E_L} \frac{I_k}{4 \cdot \pi \cdot \sigma_s} \cdot \left(\frac{1}{r_e} - \frac{1}{dist3(x, y, z, x_{e_k}, y_{e_k}, \zeta)} \right) d\zeta$$

Calculated Potential Differences

Voltage difference between active electrodes:

$$\Delta V_a := \phi\left(x_{e_1}, y_{e_1} + 1\,cm, z_{e_1} + 0.5 E_L\right) - \phi\left(x_{e_3}, y_{e_3} - 1\,cm, z_{e_3} + 0.5 E_L\right)$$

$\Delta V_a = -23.073$ V

Voltage difference between passive electrodes:

$$\Delta V_p := \phi\left(x_{e_2}, y_{e_2} + 1\,cm, z_{e_2} + 0.5 E_L\right) - \phi\left(x_{e_4}, y_{e_4} - 1\,cm, z_{e_4} + 0.5 E_L\right)$$

$\Delta V_p = -0.599$ V

Attachment B

Numerical Modeling of Electrical Parameters in Support of the Electroosmosis Tests at TFF

MEMORANDUM

Date: 8/25/99

To: Walt Mcnab

CC: W. Daily, R. Newmark

From: A. L. Ramirez

Subject: Numerical modeling of electrical parameters in support of the electro-osmosis experiment at TFF

This memorandum describes the results of numerical modeling work which calculated various electrical parameters of interest for electro-osmosis work. These calculations were performed to provide insight on the ongoing electro-osmotic experiments ongoing at the TFF site.

Approach used:

The modeling was performed using a fully 3D, finite difference forward solver which uses the conjugate gradient method to solve the matrix equations. The modeled volume was discretized using a total of 494,000 elements (95 in x and in Y, and 80 in Z). This fine level of discretization was chosen to insure accurate calculation of the electric field near the current electrodes were the gradients are steep. In the region of interest, the side of each cubical element was 0.0762 m for the simulations pertaining to the TFF site (borehole spacing of 4.2 m); for simulations assuming a 6.1 m spacing, the side of each cubical element was 0.11 m. The boundary conditions were assumed to be Newman (at the ground/air interface) and Dirichlet at the other five sides of the cube. The boundaries were located far away from the region of interest to minimize their effects on the field calculations.

Modeling Assumptions:

1) A layered, laterally homogeneous electrical resistivity structure exists at the TFF site; the resistivity values for the various layers were based on geophysical logs run on boreholes 1115, 1513, 1514, and 1515. Two different distances between the graphite electrodes were considered: 4.2 m and 6.1 m. The 4.2 m distance corresponds to the separation of the electrodes being used currently for the electro-osmosis experiments. The 6.1 m distance is the currently planned electrode separation for future remedial work. The electrode layout assumed is shown in Figure 1.

2) The resistivity structure was assumed to be unaffected by the chemical / physical changes created by the electro-osmosis process.

3) The electrodes were assumed to be made of graphite with dimensions of 3.05 m in height, and 0.076 m in diameter. The electrical resistivity of graphite can range from $10^{-6.5}$ to $10^{-1.5}$ ohm-m depending on the amount of chemical impurities, structural defects, the type of crystalline structure (Hearst and Nelson, 1985). The graphite was assumed to have an electrical resistivity of 10^{-6} ohm-m for the modeling work. At TFF, the electrodes exits within a section of the well screened with plastic. The effects of the plastic screen on the various electrical parameters was modeled by surrounding the electrodes with a resistive, square casing. The "casing" is intended to model anything other than the electrodes or the formation that affects the resistance, e.g., plastic well screen, water annulus in the well, grout

or other materials around the well screen, and mineral precipitation. The resistivity value for the casing materials was chosen such that the bulk resistance of the model would match the field measurements of bulk resistance. The approach followed to adjust the model to the bulk resistance measurements will be described later.

4) All calculations assume that 1 Amp current is flowing through the soil/electrode system.

5) The electro-osmotic velocities, V_{eo},were calculated assuming the following formula (provided by W. Mcnab):

$$V_{eo} = \frac{\kappa \Delta \phi}{n}$$

were κ is the electro-osmotic mobility and $\Delta\phi$ is the potential gradient, and n is the porosity.

The calculations assumed homogeneous porosity and electro-osmotic mobility values of 0.25 and $5.0*10^{-9}$, respectively. Future calculations could easily use heterogeneous porosity and electro-osmotic mobility values as they become available.

Comparisons of numerical results to analytical solutions:

Figure 2 shows the simulations results for the case of point electrodes separated by a distance of 4.2 m and buried at a depth of 34.7 m . The top row of images consist of vertical and horizontal slices showing the resistivity structure within the region of interest. An 8 ohm-m, homogeneous resistivity distribution is indicated in Figure 2. The horizontal plane (the rightmost image in the top row) shows a top view of the region of interest at depth of 34.7 m. The second row of images shows the same two vertical and horizontal slices: the two leftmost images show the log10 voltages, and the two rightmost images show the log10 current density along the plane coplanar with the electrodes. The bottom row of images show the total current density on the left and the electro-osmotic velocities on the right.

These simulations results can be compared to analytical solutions pertaining to voltage differences and current density. Figure 2 shows dark crosses indicating the locations were the numerical results and analytical solutions were compared. The potential field images were compared to an analytic solution for particular electrode array called the Wenner array (Telford et al., 1976). The potential field images in Figure 2 (2nd row, leftmost images) show the location of the current and voltage measurement electrodes used in a Wenner array. The Wenner array equation relates apparent resistivity , ρ_a, to voltage ΔV:

$$\Delta V = \frac{\rho_a I}{4\pi a}$$

were I is the current the distance, a, is defined in Figure 2. The apparent resistivity and the true resistivity are the same for the case of a homogeneous medium. This analytic solution yields a value of 0.46 V whereas the numerical solution equals 0.48 V.

The rightmost images in the second row of Figure 2 show the current density results along the X direction. Telford et al. indicate that the analytic solution for current density, j_x, along a vertical plane coplanar with the current electrodes is:

$$j_x = \frac{1}{4\pi}\left(\frac{x}{r_1^3} - \frac{x-L}{r_2^3}\right)$$

were x, L, r_1 and r_2 are defined in the figure. The current density calculated numerically for the location closest to the leftmost electrode is 0.45 A/m^2; the corresponding analytical solution is the same to two significant digits. The current density calculated numerically for the location that is collinear with and centered between the two electrodes is 0.36 A/m^2 and the corresponding analytical solution is 0.36. The current density for the deepest location shown in Figure 2 is 0.45 A/m^2 and the numerical solution is the same to two significant digits.

Figure 3 shows the simulation results for the case of 3.05 m tall, graphite electrodes separated by a distance of 4.2 m, and ranging in depth from 33.4 to 36.4 m. In this case, a homogeneous resistivity distribution of 8 ohm-m was used. Relative to the point electrode case (Fig. 2), the longer electrodes produce an even electric field in the vertical direction, smaller voltage gradients, and smaller current densities near the electrodes. The two leftmost images in the third row of Figure 3 show the electro-osmotic velocities. The horizontal plane shows that the velocities drop off rapidly in the direction orthogonal to the electrode plane. This figure suggests that the effective treatment distance orthogonal to the electrode plane is at best 1/2 of the electrode spacing. The change in the resulting electro-osmotic velocities between the long and point electrodes cases is shown by the two rightmost images in the third row of Figure 3. Note that near the center of the electrodes the change in electro-osmotic velocities are about -75 %. This means that the velocities are lower for the long electrode case. Conversely, near the edges of the long electrodes, the velocities have increased many hundreds of percent. Halfway between the two electrodes, however, the change in velocities is only about 10% smaller for the long electrode case. In summary, the results in Figure 3 suggest that increasing electrode length will cause large change in velocity near the electrodes and relatively small changes in velocity between the electrodes.

The next case considers the effect of resistivity heterogeneities as shown in Figure 4. The resistivity values (top row of images) were chosen from the geophysical logs in the depth range of the graphite electrodes. In general, the upper half of the electrodes is in contact with higher resistivity soil than the lower half; the contrast in resistivity is about a factor of 3. Comparisons between Figures 3 and 4 show that the region between 35 and 36.5 m depth has a higher current density; this is due to the lower resistivity of the layering in this region. The third row of images pertains to electro-osmotic velocities. The images on the right side of the this row show the changes in velocities between the homogeneous and heterogeneous cases. These images show that the electro-osmotic velocities in the resistive layers between 33.2 and 34.6 m depth increased by about 40-50% near the electrodes; halfway between the electrodes the electro-osmotic velocities increased by about 5%. In the lower resistivity layers below 36.5 m, there are decreases in velocities of about 15-20% near the electrodes, and halfway between the electrodes the velocities decreased by about 5%. In conclusion, the results in Figure 4 indicate that the modest contrast in electrical resistivity present at the TFF site results in modest variations in electro-osmotic velocities between the layers.

The results presented so far assume that the electrodes are in perfect electrical contact with the formation. We now consider the effects of the plastic screen surrounding the graphite electrodes. A priori, we expected that the plastic screen could have degraded the electrical contact between the electrodes and the formation by some unknown amount. To capture the effects of the plastic screen in the model, we chose to surround the electrodes in a resistive envelope. The value of the resistivity of this envelope was adjusted to match the bulk resistance values measured using the graphite electrodes (2 point resistance measurement). W. Mcnab and W. Daily reported resistance values ranging from 9 - 11 ohm. This means that if a 1 Amp current is flowing between the two graphite electrodes surrounded by the screen, the voltage difference between the electrodes would range from 9 to 11 V. In the model, we adjusted the resistivity value of the material around the electrodes until a voltage difference of about 10 V was observed.

The results in Figure 5 include the effects of the resistive envelope or casing surrounding the electrodes. The value of the resistive casing had to be set to 400 ohm-m in order to match the measured values of bulk resistance made in the field; this value is 25 times higher than the maximum value shown by the color bar. Note that the voltages shown by the leftmost pair of images in row 2 are about $10^{0.7}$ V (5 V) near either electrode. Given that the absolute value of the potential field is being plotted, this means that the voltage difference is 10 V. There are significant differences between the "casing" (Fig. 4) and "no casing"(Fig. 5) results. In particular the voltages and voltage gradients close to the electrodes are clearly different. Also, changes in electro-osmotic velocities can be observed. Near the electrodes and within the more resistive layers, the velocities increased by about 30 to 50 %; halfway between the electrodes the velocities are higher by 5 - 10%. Decreases in velocity of about 15% are observed in the least resistive layers close to the electrodes and about 5% decreases halfway between the electrodes. The results in Figure 5 suggest the following conclusions: 1) the effects of the plastic screen can be modeled by enclosing the electrodes within a resistive material having a resistivity (400 ohm-m) which is 50 X more resistive than the average formation resistivity (8 ohm-m), 2) the effects of adding the resistive screen to the problem are qualitatively similar to the effects of adding heterogeneity in the resistivity of the layers, and 3) higher velocities (relative to the "no casing" case are created in the more resistive layers and lower velocities are created in the least resistive layers.

An additional set of bulk resistance measurements was made in the field using a 4 electrode approach, i.e., two electrodes were used to drive current through the ground (electrodes in boreholes 1513 and 1515) and a second pair of electrodes was used to measure a voltage difference (electrodes in boreholes 1514 and 1115). We used this data as a field check on the forward solution for the voltage field. The results of this test are chown in Figure 6. The figure shows the absolute value of the potential field assuming 1 Amp of current. The calculated potential at borehole 1514 is about $10^{-1.27}$ or 0.054 V for the case that considered a 400 ohm-m casing around the electrode and the layered resistivity distribution shown in Figure 5. The calculated potential at borehole 1115 is about $10^{-1.70}$ or 0.020 V. This means that the calculated voltage difference is about 0.074 V. The resistance values reported by W. Mcnab and W. Daily were about 11 ohms or 0.11 V /Amp. This means the calculated and measured voltage differences are different by about 33%. This difference could have been easily reduced by adjusting of the electrical resistivity near the electrodes. We chose not to do this because the difference is sufficiently small to indicate that the forward solver is calculating credible voltage fields.

The electro-osmotic velocities in Figure 5 can be used to do one more check against field observations. W. Mcnab reports that during the course of electro-osmosis experiments at the site, a few gallons of water per day were recovered from the electrode wells. The electro-osmotic velocities in Figure 5 can be used to calculate the volume of water produced at the electrode well. Note that the velocities in the formation near the well are about 10^{-7} m/s. Assuming a well with a radius of 0.0762 m and a length of screen of 3.05 m, the volume of water per day is 0.012 m^3 or, 3.3 gallons/day. This comparison between calculated and observed fluxes suggests that the electro-osmotic velocities calculated are similar to those created during the field experiments.

The 3 fold contrast in resistivity observed at the TFF site is quite modest relative to our previous experience at LLNL; we have found that typical resistivity contrasts are about 10 fold. Thus, it is likely that future electro-osmosis applications may be performed on site under higher resistivity contrast conditions. This scenario is examined in Figure 7. Note that the resistivity of the most resistive layers was increased by a factor of 3 while the value of the more conductive layers remained constant. The upper row of images in the figure shows that layer contrast ranges from $10^{0.7}$ to $10^{1.7}$ ohm-m. The potential field images on the left

side of the second row indicate that higher voltage gradients are created in the high resistivity layers.

The results in Figure 7 can be compared to the 3 fold contrast results in Figure 5. The current density images (rightmost images in the second row) show that stronger current focusing is occurring in the least resistive layers. The electro-osmotic velocity images indicate much faster velocities in the resistive layers and somewhat faster velocities in the least resistive layers. Also, the horizontal plane shows that the width of the region were the velocities are 10^{-8} m/s or higher has widened considerably. The percent difference images show increases of about 300% in the resistive layer near the electrodes and about 100% increases halfway between the electrodes. In the least resistive layers, increases of about 50% near the electrodes, and of 20% halfway between the electrodes are observed. In conclusion, the effect of higher resistivity contrast is to strongly increase velocities in the high resistivity layers, and modestly increase velocity in the low resistivity layers; the higher contrasts also result in wider regions of influence. The increases in velocity in the resistive layers are caused by the steeper voltage gradients that can be maintained as the resistivity is increased. The increases in velocity in the conductive layers are caused by focusing current towards these layers and away from the resistive layers; this focusing allows steeper voltage gradients to be maintained within the conductive layers.

Current plans for future electro-osmosis deployments call for 20 ft (6.1 m) electrode separations. This scenario was also modeled and the results are shown in Figure 8. The side of each mesh element cube was increased to 0.11 m to account for the longer electrode separations. When compared to the results in Figure 5, Figure 6 shows significant decreases in the current density and electro-osmotic velocity halfway between the electrodes. The percent difference images show that halfway between the electrodes the velocities decrease 40 - 60 %.

One important aspect of any remediation treatment is its ability to provide treatment away from the emplacement boreholes. The figures shown previously indicate that electro-osmotic velocity changes horizontally between the electrodes as well as orthogonal to the electrode plane. Also, the results show that contrasts in the electrical resistivity of the layers affect electro-osmotic velocity. Figure 9 illustrates the changes in the size of the treatment volume; the figure compares the velocities calculated within high and low resistivity layers for some of the cases considered. The first column of images shows the velocities for the case with "no casing" and 3 fold contrast in resistivity. The second column of images shows the velocities for the case with a 400 ohm-m casing and 3 fold contrast in resistivity. The third column of images shows the velocities for the case with a 400 ohm-m casing and 10 fold contrast in resistivity. Comparing velocities within the first column, very little difference is observed between the high and low resistivity layers. Comparing velocities within the second column, a slight difference in the width of the velocity fields can be observed. Within the third column, a clear difference can be observed, with the resistive layer (upper row image) showing a significantly wider velocity field than the conductive layer. We can also compare the widths of the velocity fields between the different modeling scenarios; i.e., compare results within each row. This comparison indicates that the 10 fold contrast in resistivity produces the widest velocity fields for both the high and low resistivity layers.

Summary and Conclusions:

Numerical modeling work has been performed to calculate various electrical parameters which influence electro-osmotic transport. The purpose of this work is to provide insight regarding ongoing electro-osmosis experiments at TFF. The modeling was performed using a finite difference solver which calculated the electric field. The region of interest was represented by close to 0.5 million cubical elements with sides ranging from 0.0762 to 0.11 m. Several assumptions were made while performing the calculations. The most significant are: 1) the value of the resistivity assumed for the graphite electrodes was 10^{-6} ohm-m; this value could be off by a few orders of magnitude and have a significant effect on the results, 2) the effects of the plastic screen can be effectively modeled by surrounding the electrodes with elements having a high resistivity, 3) the formation's resistivity is unaffected by the chemical / physical changes created by the electro-osmosis process, and 4) homogeneous porosity and electro-osmotic mobility values were used to calculate electro-osmotic velocities; future calculations could easily use heterogeneous porosity and electro-osmotic mobility values as these are measured during ongoing investigations.

The numerical results were compared to analytical solutions and field observations of bulk resistance, voltage differences and electro-osmotic flux. The comparisons indicate that the numerical results are in reasonable agreement with the field observations and analytic solutions. The modeling scenarios considered variable electrode spacing, resistivity contrast, the presence or absence of resistive material around the electrodes, and the length of the electrodes.

Some of the most important conclusions are:

Of the variables considered, electrode spacing and resistivity contrast seem to have the largest effects on electro-osmotic velocities.

Higher resistivity contrasts increase velocities strongly in the high resistivity layers and modestly in the low resistivity layers; the higher contrasts also result in wider regions of influence. Higher contrasts also produce wider electro-osmotic velocity fields within the layers.

For the 4.2 m electrode separations, the effective treatment distance along a plane orthogonal to the electrode plane is, at best, 1/2 of the electrode spacing.

Increasing the electrode separation from 4.2 to 6.1 m will cause reductions in electro-osmotic velocities of about 50 % halfway between the electrodes.

Increasing electrode length from a point to 3.05 m will cause large change in velocity near the electrodes and relatively small changes in velocity between the electrodes.

The modest electrical resistivity contrast (3 fold) present at the TFF site results in modest variations in electro-osmotic velocities between the layers; the fastest velocities are observed near the electrodes and within the most resistive layers.

The effects of the plastic screen can be modeled by enclosing the electrodes within a resistive material having a resistivity which is 50 X more resistive than the average formation resistivity.

The effects of adding the resistive screen to the problem are qualitatively similar to the effects of adding heterogeneity in the resistivity of the layers; higher velocities (relative to the "no casing"

case) are created in the more resistive layers close to the boreholes and lower velocities are created in the least resistive layers.

A comparison between calculated and observed electro-osmotic fluxes suggests that the calculated electro-osmotic velocities are of the same order as those observed during the field experiments.

The validity of the conclusions presented above is strongly dependent on the assumptions made. As new data becomes available, these assumptions should re-assessed and the calculations should be repeated as needed.

REFERENCES:

Hearst, J. R., and P. Nelson, 1985, Well logging for physical properties, McGraw Hill Book Co. New York.

Telford, W., L. Geldart, R. Sheriff, and D. Keys, 1976, Applied Geophysics, Cambridge University Press, Cambridge, UK.

ALR/ALR

9 figures as attachments

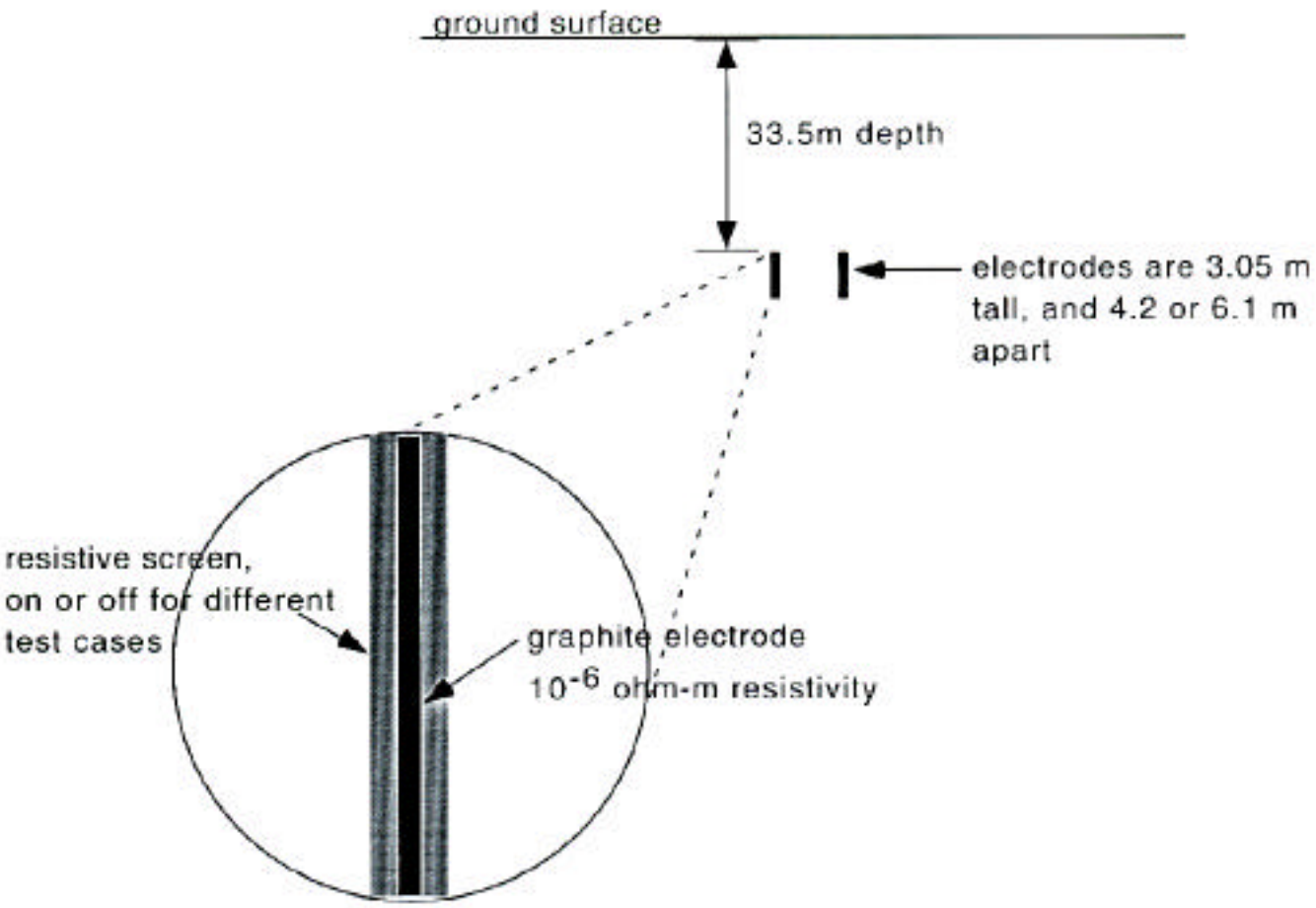

Figure 1 shows the electrode layout assumed for the modeling study.

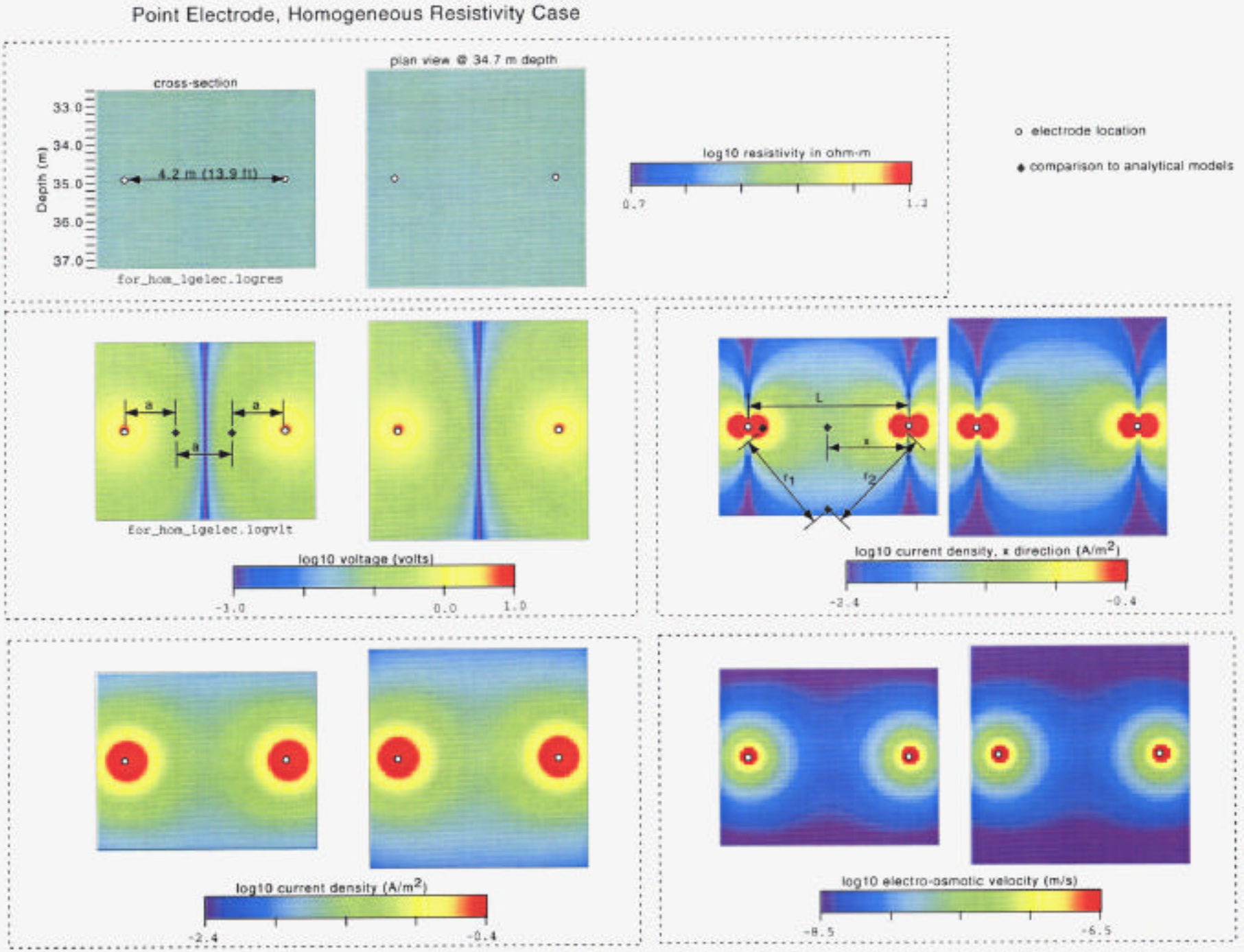

Figure 2 shows the values of various electrical parameters along vertical and horizontal slice. The location of the horizontal slice is at a depth of 34.7 m. This simulation assumed a homogeneous resistivty distribution and point electrodes. The results were compared to analytical solutions to evaluate the accuracy of the forward solver; the locations where the comparisons were performed are indicated by black crosses. The values shown are LOG10 values of voltage, current density, current density in the X direction, and electro-osmotic velocity.

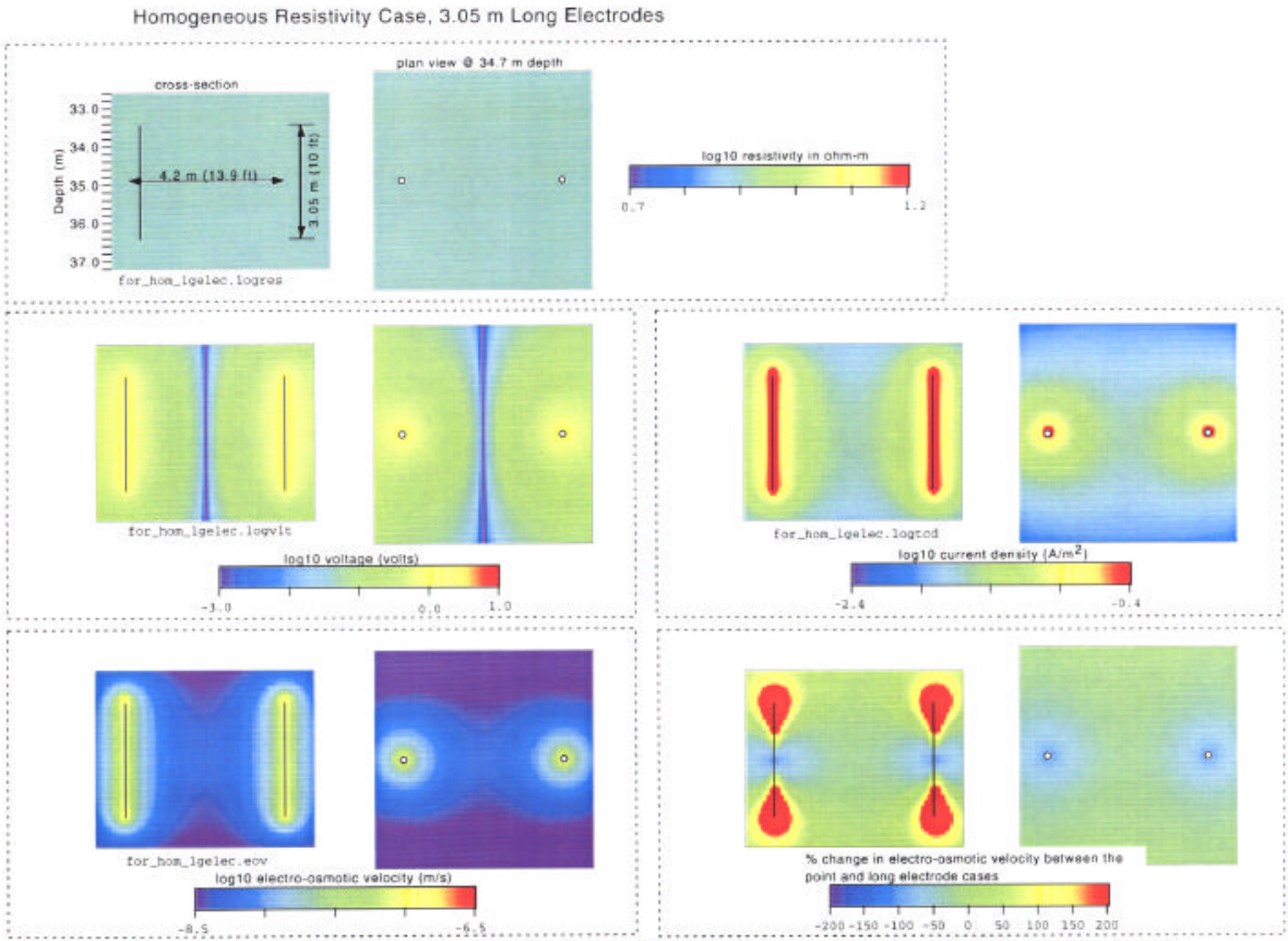

Figure 3 shows the values of various electrical parameters assuming a homogeneous resistivity distribution and 3.05 m tall graphite electrodes. The resistivity value chosen (8 ohm-m) is the average resistivity measured by the geophysical logs in the depth range of the electrodes. The values shown are LOG10 values of voltage, current density, and electro-osmotic velocity. The percent differences in electro-osmotic velocities illustrate the effects of increasing the length of the electrodes to 3.05 m.

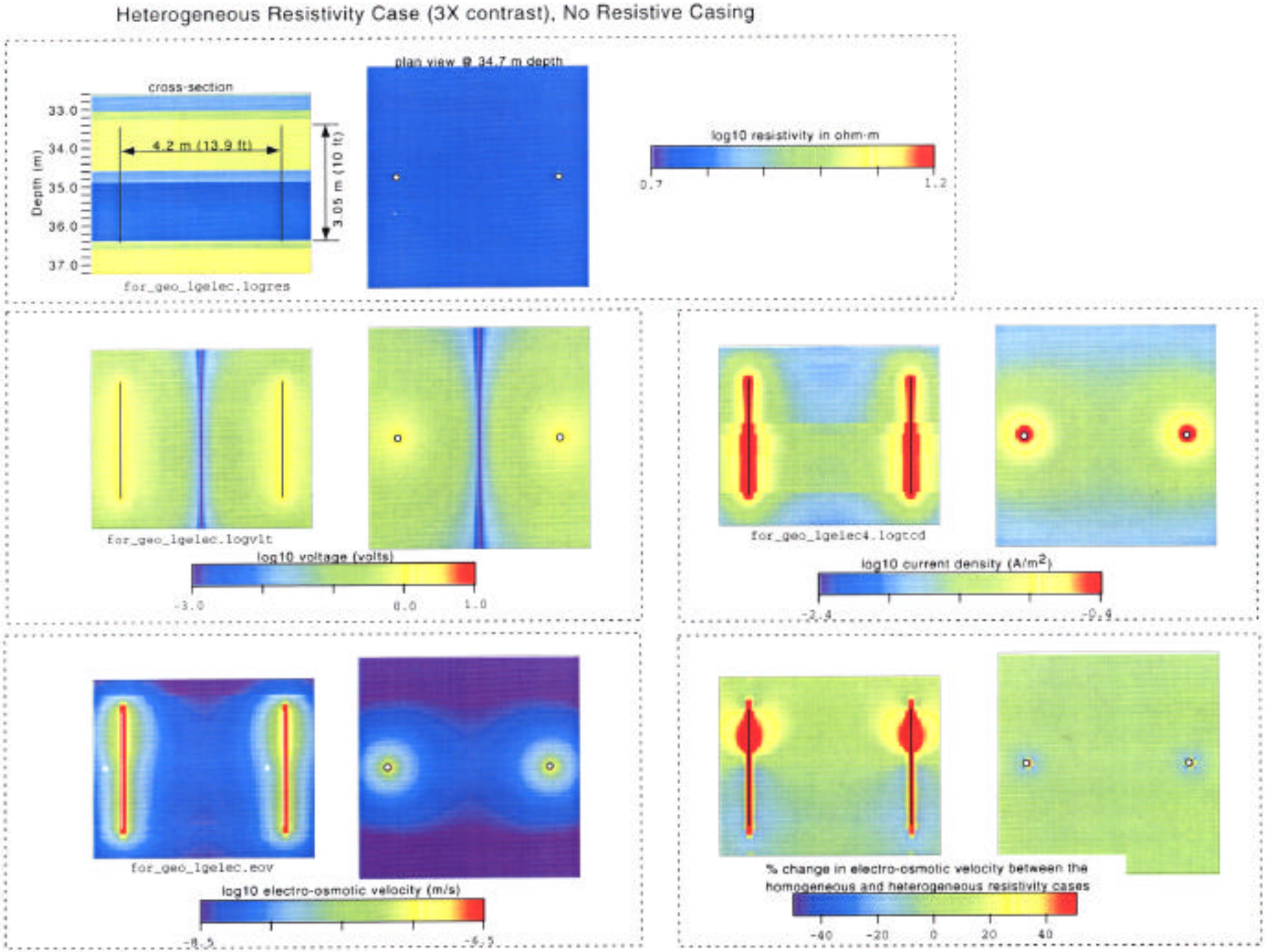

Figure 4 shows the values of various electrical parameters assuming a heterogeneous resistivty distribution with a three fold contrast, and 3.05 m tall graphite electrodes. The resistivity values were chosen from the geophysical logs in the depth range of the electrodes. The values shown are LOG10 values of voltage, current density, and electro-osmotic velocity. The changes in electro-osmotic velocities shown are caused by changing from a homogeneous to a heterogeneous resistivity distribution.

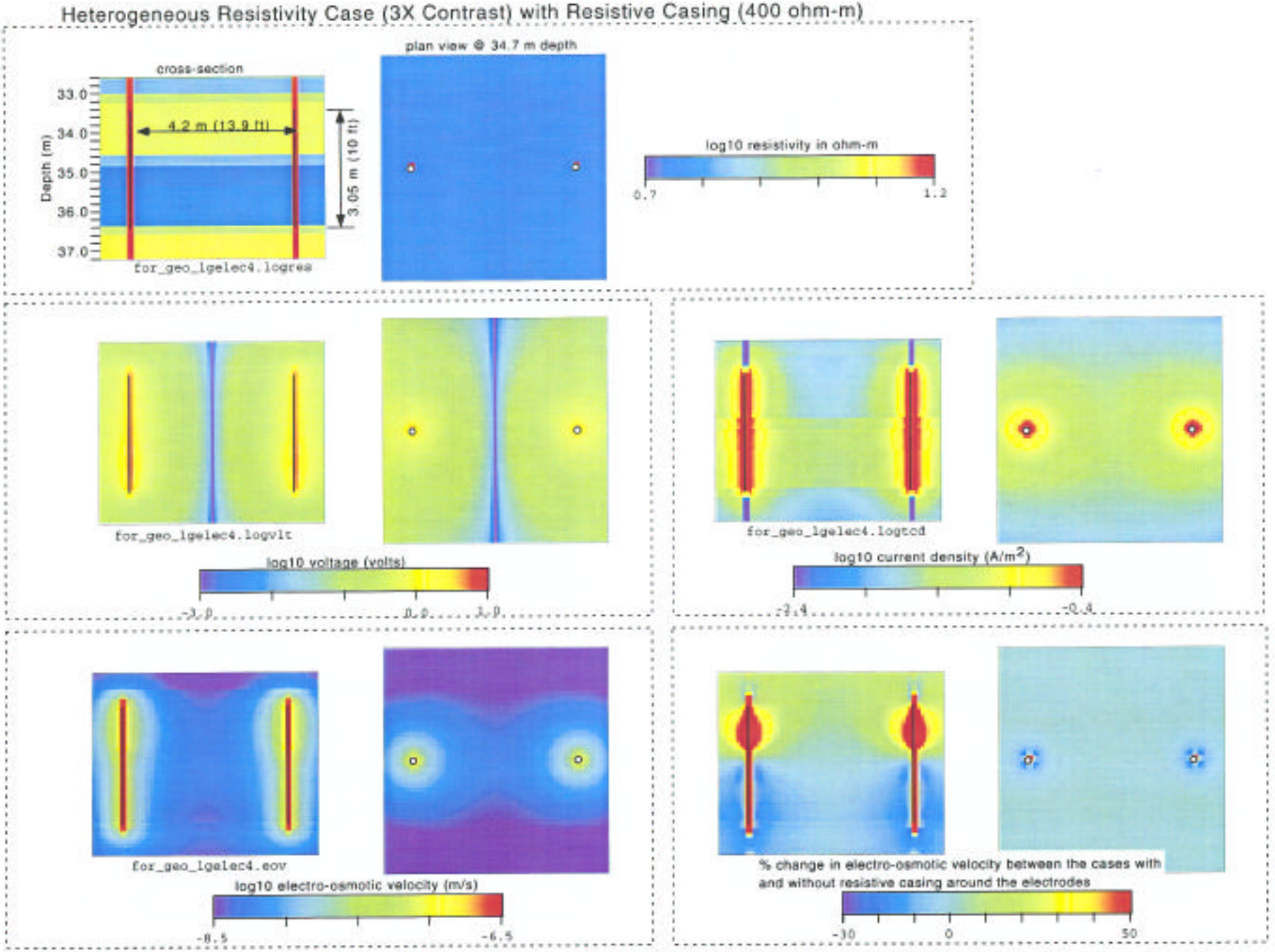

Figure 5 shows the values of various electrical parameters assuming a heterogeneous resistivity distribution with a 3 fold contrast, 3.05 m tall graphite electrodes and a resistive casing around the electrodes. The resistivity values were chosen from the geophysical logs in the depth range of the electrodes. The values shown are LOG10 values of voltage, current density, electro-osmotic velocity, and percent differences in electro-osmotic velocities relative to the velocities in Figure 4; these percent differences illustrate the effect of adding the resistive casing to the model.

Voltage test assuming heterogeneous resistivity case (3X Contrast) with resistive casing (400 ohm-m)

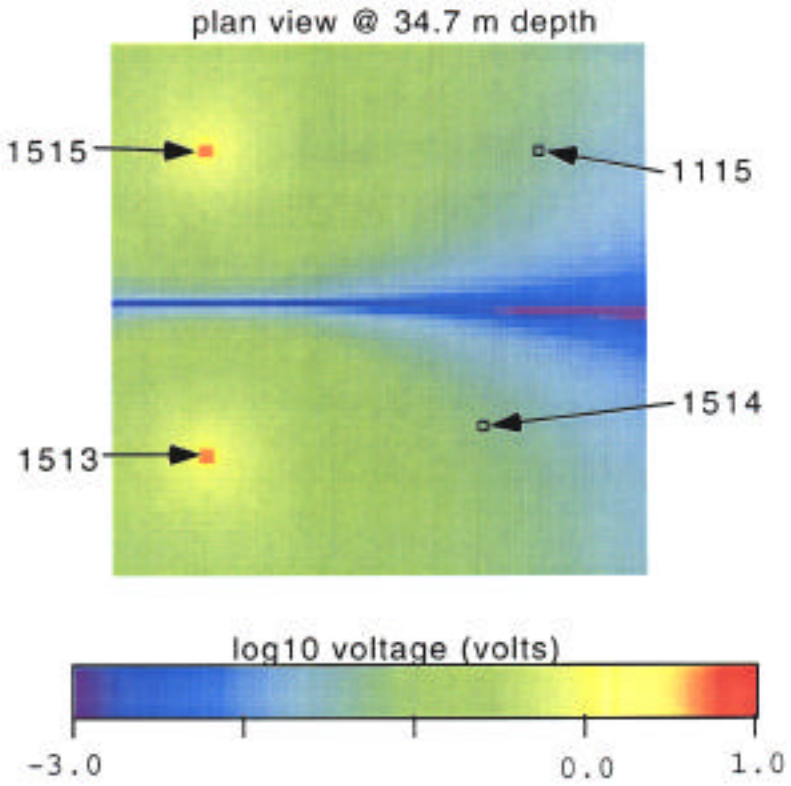

potential @ 1115 = $10^{-1.698}$ = 0.02 V

potential @ 1514 = $10^{-1.269}$ = 0.054 V

delta V (1115 - 1514) = 0.074 V, field measurements indicate 0.11 V

Figure 6 shows the potential field calculated when electrodes in boreholes 1515 and 1513 are used as current electrodes to inject 1 Amp of current. Electrodes in boreholes 1115 and 1514 are used to measure a potential difference. The comparison between the measured and calculated values is also indicated.

Heterogeneous Resistivity Case (10X contrast) with Resistive Casing (400 ohm-m)

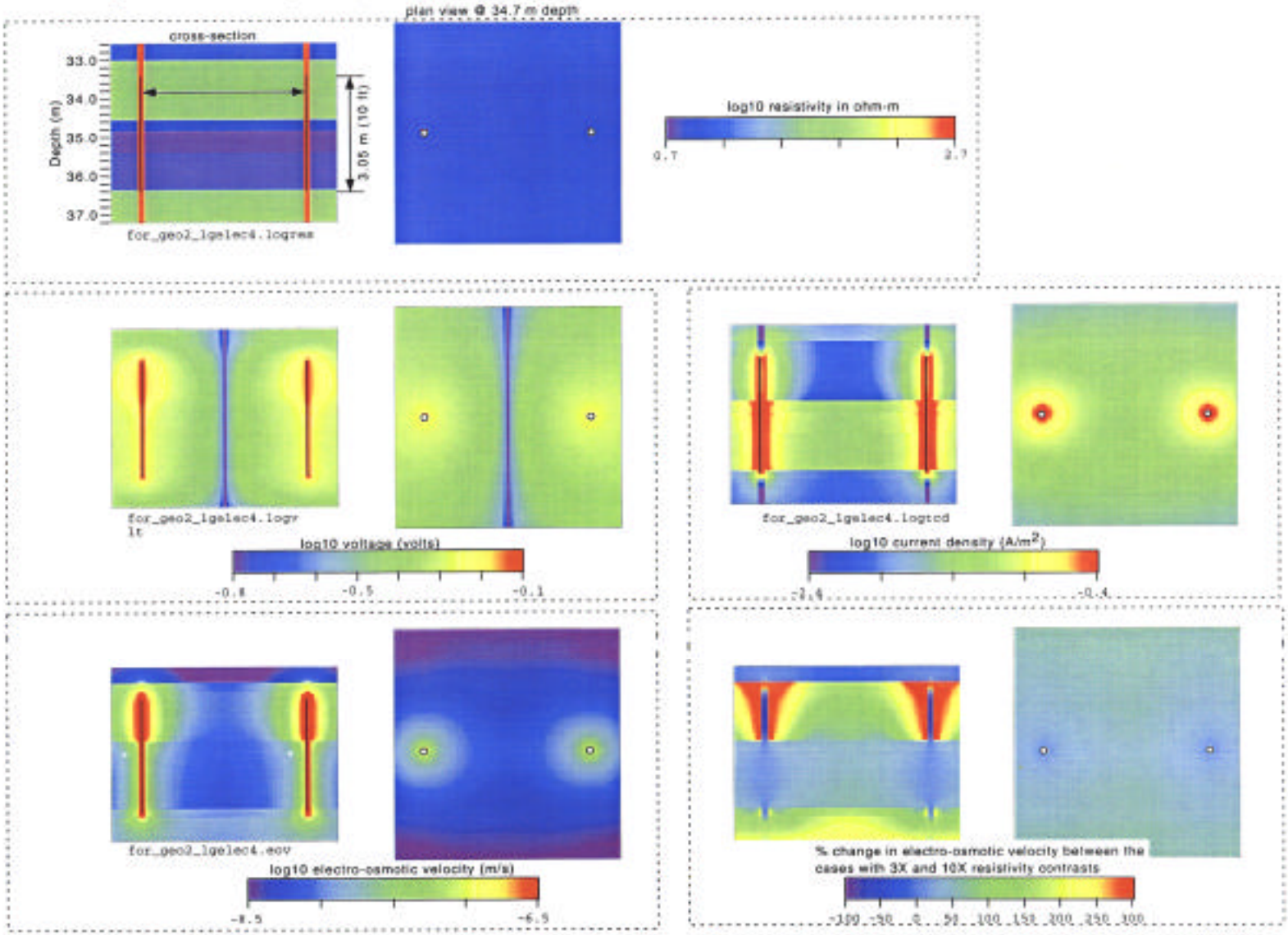

Figure 7 shows the values of various electrical parameters assuming a heterogeneous resistivity distribution, 3.05 m tall graphite electrodes and a resistive casing around the electrodes. The resistivity values of the higher resistivity layers was increased to provide a contrast of about tenfold. The values shown are LOG10 values of voltage, current density, electro-osmotic velocity, and percent differences in electro-osmotic velocities relative to the velocities in Figure 5; these percent differences illustrate the effect of higher resistivity contrasts on the velocities.

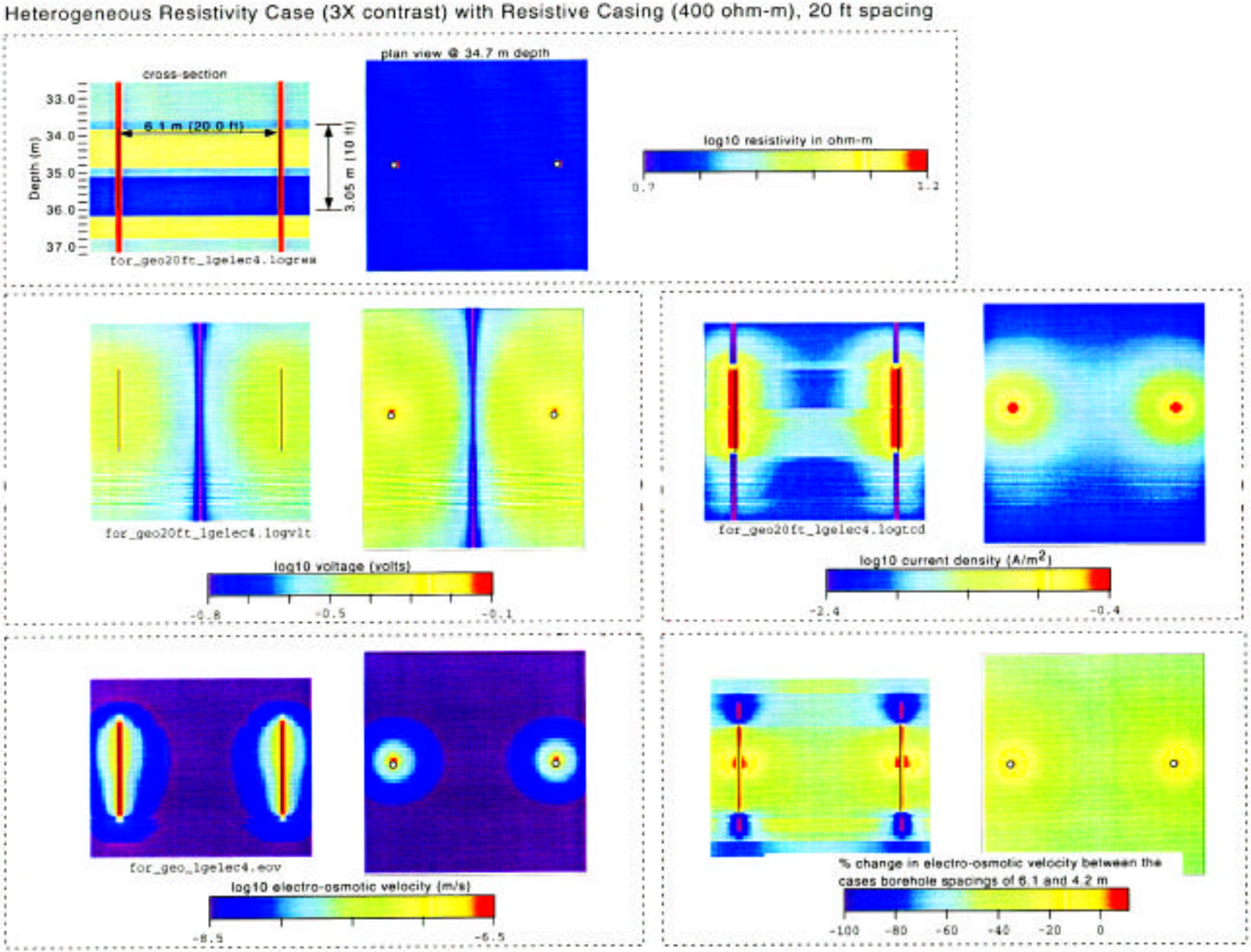

Figure 8 shows the values of various electrical parameters assuming a longer (6.1 m) borehole separation, a heterogeneous resistivty distribution, 3.05 m tall graphite electrodes and a resistive casing around the electrodes. The resistivity values of the resistive layers was increased to provide a contrast of about tenfold. The values shown are LOG10 values of voltage, current density, electro-osmotic velocity, and percent differences in electro-osmotic velocities relative to the velocities in Figure 5; these percent differences illustrate the effect of longer electrode spacings on the velocities.

Attachment C

Semi-Analytical Model of Voltage Distribution and Electroosmotic Flux

Electroosmosis Screening Model

This 3-D model is based upon the assumption that the electric field may be defined using simple potential theory. Cathodes and anodes are modeled as electron sources and sinks, respectively, using a continuous point source solution in an infinite homogeneous 3-D domain. Point sources are then integrated in the vertical direction to simulate a continuous line source (i.e. finite lengt electrode). The groundwater velocity vector field is calculated using an analogy to Darcy's law, where water flow in response to the voltage gradient in a rate proportional to the electroosmotic conductivity coefficient (as measured in the laboratory). This assumes that the hydraulic head distribution is hydrostatic (i.e. there are no driving forces for groundwater flow other than the electric field).

Sediment Properties

$\sigma_s := 0.128 \frac{S}{m}$ (electric conductivity - based on best fit to 4-electrode resistivity test)

$k_{eo} := 2.3 \cdot 10^{-9} \frac{m^2}{sec \cdot V}$ (electroosmotic conductivity - best fit to measured electroosmotic flux)

$\eta := 0.30$ (porosity - assumed)

EO System Properties

$E_L := 10 ft$ (electrode length)

$E_d := 3 in \qquad r_e := \frac{E_d}{2}$ (electrode diameter and radius)

$E_A := \pi \cdot r_e \cdot (2 \cdot E_L + r_e)$ (electrode surface area)

Electrode configuration (elevation with reference to bottom of electrode):

$N := 4$ (total number of electrodes)

ORIGIN := 1 (set first array index = 1)

Geometrical arrangement of electrodes is based on a regular grid, constrained by the given spacings in the x- and y-directions.

$c_e := \begin{bmatrix} 0.0 \\ 0.0 \\ -120 \end{bmatrix}$ ft (location of reference cathode)

$\Delta x := 10\text{ft}$ (east-west spacing) $\Delta y := 10\text{ft}$ (north-south spacing)

$x_e := \begin{bmatrix} c_{e_1} \\ c_{e_1} + \Delta x \\ c_{e_1} \\ c_{e_1} + \Delta x \end{bmatrix}$ $y_e := \begin{bmatrix} c_{e_2} \\ c_{e_2} \\ c_{e_2} + \Delta y \\ c_{e_2} + \Delta y \end{bmatrix}$ $z_e := \begin{bmatrix} c_{e_3} \\ c_{e_3} \\ c_{e_3} \\ c_{e_3} \end{bmatrix}$ $I := \begin{bmatrix} 4.0 \\ 0.0 \\ 0.0 \\ -4.0 \end{bmatrix}$ amp

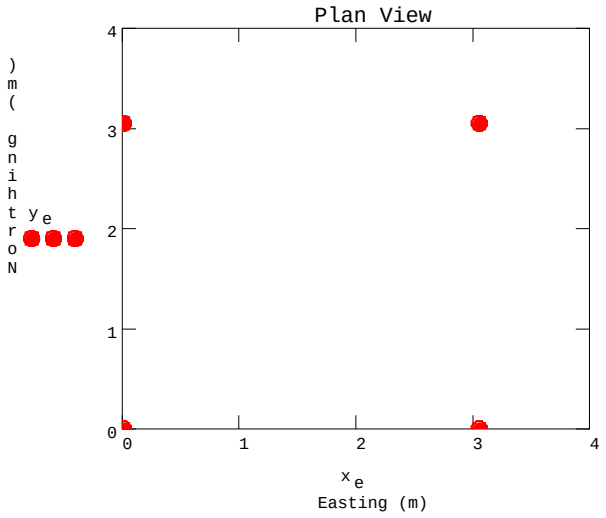

Potential Field Equations

Distance equation in 3-D:

$$dist3(x_1, y_1, z_1, x_2, y_2, z_2) := \sqrt{(x_1 - x_2)^2 + (y_1 - y_2)^2 + (z_1 - z_2)^2}$$

Potential distribution:

$$\phi(x, y, z) := \sum_{k=1}^{N} \frac{1}{E_L} \cdot \int_{z_{e_k}}^{z_{e_k} + E_L} \frac{I_k}{4 \cdot \pi \cdot \sigma_s} \cdot \left(\frac{1}{r_e} - \frac{1}{dist3(x, y, z, x_{e_k}, y_{e_k}, \zeta)} \right) d\zeta$$

Current density function:

$$\Phi(x, y, z) := \sqrt{\left(\frac{d}{dx}\phi(x, y, z)\right)^2 + \left(\frac{d}{dy}\phi(x, y, z)\right)^2 + \left(\frac{d}{dz}\phi(x, y, z)\right)^2}$$

$$\Gamma(x, y, z) := \sigma_s \cdot \Phi(x, y, z)$$

Groundwater velocity field:

$$v(x, y, z) := \begin{bmatrix} \frac{-k_{eo}}{\eta} \cdot \frac{d}{dx}\phi(x, y, z) \\ \frac{-k_{eo}}{\eta} \cdot \frac{d}{dy}\phi(x, y, z) \\ \frac{-k_{eo}}{\eta} \cdot \frac{d}{dz}\phi(x, y, z) \end{bmatrix}$$

Induced Groundwater Flux to Cathode

Volumetric flux of water to a cathode:

(1) Define a function describing the normal vector to a vertical cylinder surrounding the cathode.

$$cndr(x,y,z) := \begin{bmatrix} x_{e_1} - x \\ y_{e_1} - y \\ 0 \end{bmatrix} \qquad n(x,y,z) := \frac{cndr(x,y,z)}{\sqrt{cndr(x,y,z) \cdot cndr(x,y,z)}}$$

(2) Find component of groundwater velocity vector normal to cylinder (dot product).

$$v_n(x,y,z) := v(x,y,z) \cdot n(x,y,z)$$

(3) Evaluate surface integral about encompassing cylinder.

$\rho := 2\,ft$ (radius of cylinder encompassing cathode)

$$Q := E_L \cdot \int_0^{2\cdot\pi} \eta \cdot v_n\left(x_{e_1} + \rho \cdot \cos(\theta), y_{e_1} + \rho \cdot \sin(\theta), z_{e_1} + \frac{E_L}{2}\right) \cdot \rho \, d\theta$$

$Q = 1.553 \frac{gal}{day}$ (flux assuming horizontal flow only)

Attachment D

Semi-Analytical Model of Operational Scale Electroosmotic Groundwater Remediation in Fine-Grained Sediments

Electroosmosis Screening Model

This 3-D model is based upon the assumption that the electric field may be defined using simple potential theory. Cathodes and anodes are modeled as electron sources and sinks, respectively, using a continuous point source solution in an infinite homogeneous 3-D domain. Point sources are then integrated in the vertical direction to simulate a continuous line source (i.e. finite length electrode). The groundwater velocity vector field is calculated using an analogy to Darcy's law, where water flow in response to the voltage gradient in a rate proportional to the electroosmotic conductivity coefficient (as measured in the laboratory). This assumes that the hydraulic head distribution is hydrostatic (i.e. there are no driving forces for groundwater flow other than the electric field).

Sediment Properties

$\sigma_s := 0.128 \frac{S}{m}$ (electric conductivity)

$k_{eo} := 2.3 \cdot 10^{-9} \frac{m^2}{sec \cdot V}$ (electroosmotic conductivity)

$\eta := 0.30$ (porosity)

EO System Properties

$E_L := 10 ft$ (electrode length)

$E_d := 3 in$ $r_e := \frac{E_d}{2}$ (electrode diameter and radius)

$E_A := \pi \cdot r_e \cdot (2 \cdot E_L + r_e)$ (electrode surface area)

Electrode configuration (elevation with reference to bottom of electrode):

$N := 4$ (total number of electrodes)

$ORIGIN := 1$ (set first array index = 1)

Geometrical arrangement of electrodes is based on a fence configuration, with a row of anodes facing a row of cathodes.

$$c_e := \begin{bmatrix} 100.9 \\ 100.9 \\ -120 \end{bmatrix} ft$$ (location of reference cathode)

$\Delta x := 15ft$ (east-west spacing) $\Delta y := 15ft$ (north-south spacing)

$$x_e := \begin{bmatrix} c_{e_1} \\ c_{e_1} + \Delta x \\ c_{e_1} \\ c_{e_1} + \Delta x \end{bmatrix} \quad y_e := \begin{bmatrix} c_{e_2} \\ c_{e_2} \\ c_{e_2} + \Delta y \\ c_{e_2} + \Delta y \end{bmatrix} \quad z_e := \begin{bmatrix} c_{e_3} \\ c_{e_3} \\ c_{e_3} \\ c_{e_3} \end{bmatrix} \quad I := \begin{bmatrix} 15 \\ -15 \\ 15 \\ -15 \end{bmatrix} amp$$

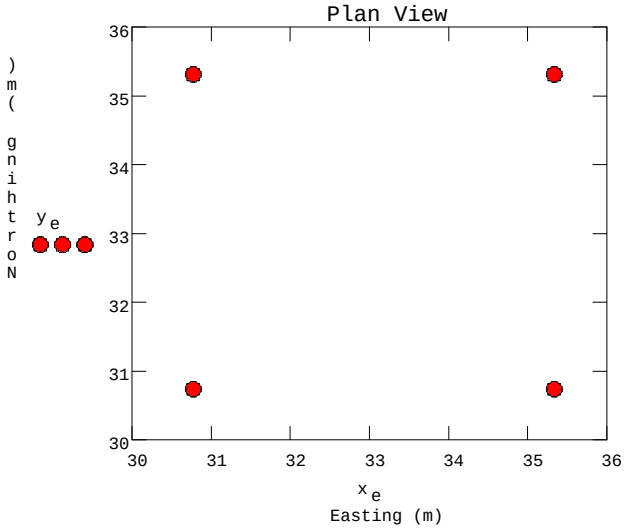

Potential Field Equations

Distance equation in 3-D:

$$dist3(x_1, y_1, z_1, x_2, y_2, z_2) := \sqrt{(x_1 - x_2)^2 + (y_1 - y_2)^2 + (z_1 - z_2)^2}$$

Anode (sink for electrons):

$$\phi(x, y, z) := \sum_{k=1}^{N} \frac{1}{E_L} \cdot \int_{z_{e_k}}^{z_{e_k} + E_L} \frac{I_k}{4 \cdot \pi \cdot \sigma_s} \cdot \left(\frac{1}{r_e} - \frac{1}{dist3(x, y, z, x_{e_k}, y_{e_k}, \zeta)} \right) d\zeta$$

Gradient equations (used to override MathCad $r\delta := 1\,cm$):

$$grad\phi_x(x, y, z) := \frac{(\phi(x + 0.5\delta, y, z) - \phi(x - 0.5\delta, y, z))}{\delta}$$

$$grad\phi_y(x, y, z) := \frac{(\phi(x, y + 0.5\delta, z) - \phi(x, y - 0.5\delta, z))}{\delta}$$

$$grad\phi_z(x, y, z) := \frac{(\phi(x, y, z + 0.5\delta) - \phi(x, y, z - 0.5\delta))}{\delta}$$

Induced Groundwater Movement

Groundwater velocity field:

$$v(x, y, z) := \begin{bmatrix} \frac{-k_{eo}}{\eta} \cdot grad\phi_x(x, y, z) \\ \frac{-k_{eo}}{\eta} \cdot grad\phi_y(x, y, z) \\ \frac{-k_{eo}}{\eta} \cdot grad\phi_z(x, y, z) \end{bmatrix}$$

Particle Travel Time

Time step size: $\Delta t := 97\,day$ Number of time steps: $n_t := 20$

End time: $t_f := n_t \Delta t$ $t_f = 5.312\,yr$

Explicit finite-difference approximation for particle migration: $iter = 1 .. n_t$

Initial conditions:

$$\begin{bmatrix} t_1 \\ x1_{iter} \\ y1_{iter} \\ z1_{iter} \end{bmatrix} := \begin{bmatrix} 0\,day \\ xe_1 + 0.5\,\Delta x \\ ye_1 + 0.5\,\Delta y + 1\,ft \\ ze_1 + 0.5\,H_L \end{bmatrix}$$

Finite difference solution:

$$\begin{bmatrix} t_{iter+1} \\ x1_{iter+1} \\ y1_{iter+1} \\ z1_{iter+1} \end{bmatrix} := \begin{bmatrix} t_{iter} + \Delta t \\ x1_{iter} + \Delta t \cdot v(x1_{iter}, y1_{iter}, z1_{iter})_1 \\ y1_{iter} + \Delta t \cdot v(x1_{iter}, y1_{iter}, z1_{iter})_2 \\ z1_{iter} + \Delta t \cdot v(x1_{iter}, y1_{iter}, z1_{iter})_3 \end{bmatrix}$$

Effective mean velocity: $\frac{dist3D(x1_1, y1_1, z1_1, x1_{n_t}, y1_{n_t}, z1_{n_t})}{t_{n_t} - t_1} = 0.056\,\frac{in}{day}$

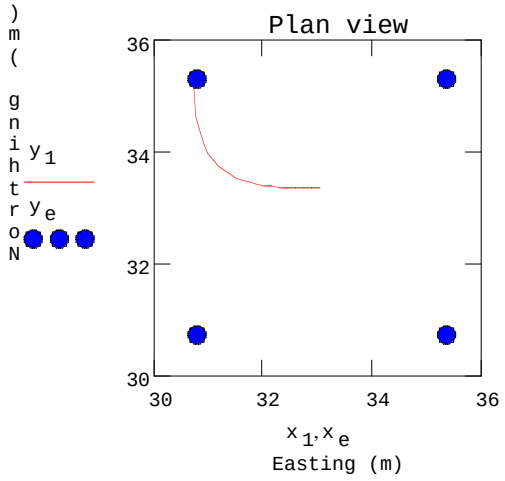

Operational Summary

Potential difference across example anode-cathode set:

$$\Delta V := \phi\left(x_{e_2} - 1\,\text{cm}, y_{e_2}, z_{e_2} + 0.5\,L\right) - \phi\left(x_{e_1} + 1\,\text{cm}, y_{e_1}, z_{e_1} + 0.5\,L\right)$$

$$\Delta V = 67.1\,\text{kV}$$

Per electrode pair power consumption:

$$P := I_1 \cdot \Delta V$$

$$P = 1.00\,\text{kW}$$

Attachment E

Semi-Analytical Model of Comparative Hydraulic Pumping in Fine-Grained Sediments

Pumping Model in 3-D

This 3-D model is based upon point sources and sinks for water withing a homogeneous, infinite 3-D aquifer. Point sources are converted to line sources by integrating in the vertical direction.

Aquifer Properties

$K := 1 \cdot 10^{-8} \frac{cm}{sec}$ (hydraulic conductivity)

$\eta := 0.30$ (porosity)

Coupled Extraction/injection Well System

$r_w := 3\,in$ (pumping well radius)

$S_L := 10\,ft$ (length of screened interval)

Electrode configuration (elevation with reference to bottom of well screen):

$N := 4$ (total number of wells)

$ORIGIN := 1$ (set first array index = 1)

Geometrical arrangement of wells is based on a fence configuration, with a row of injection wells facing a row of extraction wells.

$c_w := \begin{bmatrix} 100.9 \\ 100.9 \\ -120 \end{bmatrix} ft$ (location of reference well)

$\Delta x := 15\,ft$ (east-west spacing) $\Delta y := 15\,ft$ (north-south spacing)

$x_w := \begin{bmatrix} c_{w_1} \\ c_{w_1} + \Delta x \\ c_{w_1} \\ c_{w_1} + \Delta x \end{bmatrix}$ $y_w := \begin{bmatrix} c_{w_2} \\ c_{w_2} \\ c_{w_2} + \Delta y \\ c_{w_2} + \Delta y \end{bmatrix}$ $z_w := \begin{bmatrix} c_{w_3} \\ c_{w_3} \\ c_{w_3} \\ c_{w_3} \end{bmatrix}$ $Q := \begin{bmatrix} 1 \cdot 10^{-4} \\ -1 \cdot 10^{-4} \\ 1 \cdot 10^{-4} \\ -1 \cdot 10^{-4} \end{bmatrix} \frac{gal}{min}$

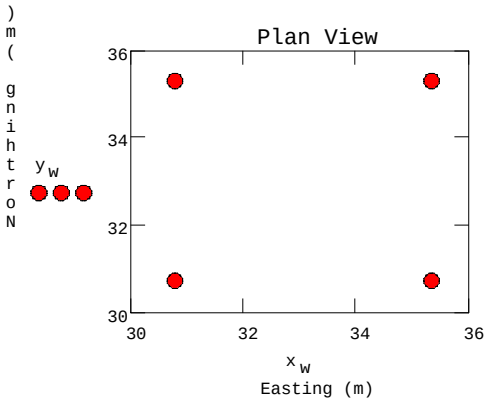

$$Q = \begin{bmatrix} 0.144 \\ -0.144 \\ 0.144 \\ -0.144 \end{bmatrix} \frac{gal}{day}$$

Potential Field Equations

Distance equation in 3-D:

$$dist3d(x_1, y_1, z_1, x_2, y_2, z_2) := \sqrt{(x_1 - x_2)^2 + (y_1 - y_2)^2 + (z_1 - z_2)^2}$$

Hydraulic potential (negative sign for Q needed to offset negative integration limits):

$$\phi(x, y, z) := \sum_{l=1}^{N} \frac{1}{S_L} \cdot \int_{z_{w_l}}^{z_{w_l} + S_L} \frac{Q_l}{4 \cdot \pi \cdot K} \cdot \left(\frac{1}{r_w} - \frac{1}{dist3d(x, y, z, x_{w_l}, y_{w_l}, \zeta)} \right) d\zeta$$

Gradient equations (used to override MathCad $r\delta := 1\,cm$):

$$grad\phi_x(x, y, z) := \frac{(\phi(x + 0.5\delta, y, z) - \phi(x - 0.5\delta, y, z))}{\delta}$$

$$grad\phi_y(x, y, z) := \frac{(\phi(x, y + 0.5\delta, z) - \phi(x, y - 0.5\delta, z))}{\delta}$$

$$grad\phi_z(x, y, z) := \frac{(\phi(x, y, z + 0.5\delta) - \phi(x, y, z - 0.5\delta))}{\delta}$$

Induced Groundwater Movement

Groundwater velocity field: $v(x,y,z) := \begin{bmatrix} -\frac{K}{\eta}\cdot \text{grad}_x(x,y,z) \\ -\frac{K}{\eta}\cdot \text{grad}_y(x,y,z) \\ -\frac{K}{\eta}\cdot \text{grad}_z(x,y,z) \end{bmatrix}$

Particle Travel Time

Time step size: $\Delta t := 4150\,\text{day}$ Number of time steps: $n_t := 20$

End time: $t_f := n_t \Delta t$ $t_f = 227.249\,\text{yr}$

Explicit finite-difference approximation for particle migration: $iter := 1 .. n_t$

Initial conditions: Finite difference solution:

$$\begin{bmatrix} t_1 \\ x1_{iter} \\ y1_{iter} \\ z1_{iter} \end{bmatrix} := \begin{bmatrix} 0\,\text{day} \\ x_{w_1} + 0.5\Delta x \\ y_{w_1} + 0.5\Delta y + 1\,\text{ft} \\ z_{w_1} + 0.5 S_L \end{bmatrix} \quad \begin{bmatrix} t_{iter+1} \\ x1_{iter+1} \\ y1_{iter+1} \\ z1_{iter+1} \end{bmatrix} := \begin{bmatrix} t_{iter} + \Delta t \\ x1_{iter} + \Delta t \cdot v_1\left(x1_{iter}, y1_{iter}, z1_{iter}\right) \\ y1_{iter} + \Delta t \cdot v_2\left(x1_{iter}, y1_{iter}, z1_{iter}\right) \\ z1_{iter} + \Delta t \cdot v_3\left(x1_{iter}, y1_{iter}, z1_{iter}\right) \end{bmatrix}$$

Effective mean velocity $= \frac{dist3d\left(x_{1_1}, y_{1_1}, z_{1_1}, x_{1_{n_t}}, y_{1_{n_t}}, z_{1_{n_t}}\right)}{t_{n_t} - t_1} = 1.3 \cdot 10^{-3}\ \frac{in}{day}$

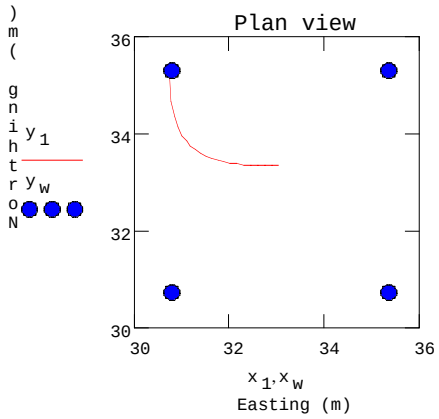

Required Head Differences Between Extraction and Injection Well Pair

$\Delta h := \phi\left(x_{w_2} - 1\,cm, y_{w_2}, z_{w_2} + 0.5 S_L\right) - \phi\left(x_{w_1} + 1\,cm, y_{w_1}, z_{w_1} + 0.5 S_L\right)$

$\Delta h = 118.560\ ft$